Variations of the sea-level muon flux

P V O'Connor

O'Connor, P V (1961) Variations of the sea-level muon flux. Masters thesis, Durham University.

Variations of the Sea-Level Muon Flux

by

P. V. O'Connor

Presented in candidature for the degree of
Master of Science of the University of Durham

Easter 1961

Preface

A solid iron magnet has been constructed under the direction of the author, in the form of a rectangular transformer core with excitation windings on opposite sides of the core. The design is based on the results of model experiments by Bennet and Nash (1960). The author was responsible for the study of the magnetic parameters of the instrument; the results have been published by the author and Dr. A.W. Wolfendale in Nuovo Cimento (1960).

The first three months of operation and interpretation of the data from the Cosmic Ray Spectrograph incorporating the above magnet were the main responsibility of the author, the result of which had been presented in a preliminary form by the author and Dr. A.W. Wolfendale in an A.R.D.C. Technical Report (1960). They are more fully treated in this thesis.

O'CONNOR, P.V., and WOLFENDALE, A.W., 1960,
Suppl. Nuovo Cimento, 15, 202.

O'CONNOR, P.V., and WOLFENDALE, A.W., 1960,
Technical Note NR 1.
Contract NR AF 61(052) - 27.
A.R.D.C., U.S.A.F.

CONTENTS

Page

List of Figures 1

List of Tables 3

Chapter 1. GENERAL INTRODUCTION 4

Chapter 2. VARIATIONS IN THE INTENSITY OF THE -MESON COMPONENT AT SEA LEVEL.......... 9

2.1. Historical Introduction 9

2.2. The Equation of Duperier 10

2.3. More Accurate analyses of the Meteorological Effects 11

2.4. Experimental Studies of the Variations as a function of Momenta 12

2.5. The Experiments of Glaser et al (1950).. 13

2.6. The requirements of an Instrument to study Flux Variations 15

Chapter 3. DESIGN AND CONSTRUCTION OF SOLID IRON MAGNET 16

3.1. General Considerations of Design 16

3.2. The Magnetic Material 18

3.3. Results of Model Experiments 21

3.4. Design and Construction of full-scale Magnet 22

3.5. The Excitation of the Magnet 24

3.6. Later Modifications for Measurements on Horizontal Cosmic Rays 25

Page

Chapter 4. MEASUREMENTS ON THE MAGNET 27

4.1. The Parameters under Investigation 27

4.2. The Fluxmeter 30

4.3. The Variation of Magnetic Flux with Time 31

4.4. The Variation of Magnetic Flux with Group Number 33

4.5. The Variation of Magnetic Flux along the OX Axis 36

4.6. The Measurement of the Leakage Flux 36

4.6a. Variation of leakage flux with height ... 36

4.6b. Variation of integral field strength over the useful area of the maget 37

4.6c. The Direction of the magnetic induction inside the magnet 38

Chapter 5. THE CHARACTERISTICS OF THE SPECTROGRAPH . 41

5.1. The Geometrical Arrangement 41

5.2. The Acceptance Function of the Spectrograph 42

5.3. The Effect of Momentum Loss on the Acceptance Function 47

5.4. The Effect of Scattering on the Acceptance Function 53

5.5. The Momentum Spectra for Various Categories 55

Page

Chapter 6. THE ELECTRONIC CIRCUITS 58

6.1. The 'Vertical Spectrograph' 58

6.2. Modifications for Horizontal Recording .. 59

Chapter 7. THE EXPERIMENTAL RESULTS ON INTENSITY VARIATIONS IN THE VERTICAL DIRECTION 61

7.1. The Basic Data on Particle Rates 62

7.2. The Meteorological Data 63

7.3. The Day-Night Particle Rate for Each Category 65

Chapter 8. CORREOLATION OF THE INTENSITY VARIATIONS WITH METEOROLOGICAL PARAMETERS 68

8.1. General Considerations 68

8.2. Correolation with pressure 68

8.3. Application of the Correolation treatment of Dorman 69

8.4. Conclusions 73

Acknowledgments 74

References 75

LIST OF FIGURES

Fig. No.	Title
1.	Relevant portion of hysterisis loop for B.5.24, Part 6. Spec. 18.
2.	General design of the magnet.
3.	Finalised design of the Solid Iron Magnet
4.	Re-designed framework for horizontal experiment.
5.	Variation of Magnetic Flux in the Magnet with Excitation Current.
6.	Variation of Magnetic Flux in the Magnet with Group Number.
7.	The mean induction as a function of plate number of group C2.
8.	Variation of Magnetic Flux along the OX axis of the magnet.
9.	Variation of leakage flux with height above the magnet.
10.	Variation of leakage flux over the useful area of the magnet.
11.	Vector diagram of horizontal component of leakage flux on surface of magnet.
12.	Variation of total flux over useful area of magnet.
13.	Dimensions of spectrograph.

Fig. No.	Title
14.	Acceptance diagrams.
15.	Acceptance curves.
16.	Variation of path through magnet due to energy loss.
17.	Scattering in solid iron spectrograph.
18.	Momentum spectra.
19.	Block diagram of circuits.
20.	Coincidence circuit.
21.	Message register circuit and quenching unit circuit.
22.	Timing circuit.
23.	Horizontal recording; Coincidence circuit for recording of shower component.
24.	Frequency distribution of intervals between particles.
25.	Meteorological stations 'near' Durham.
26.	The variation of rate with pressure.
27.	Variation of pressure coefficient with momentum.
28.	The variation of $W_T(h)$ with h.
29.	Corrected values of $_p$ as a function of momentum.

LIST OF TABLES

Table No. Title

1. The Diurnal Variation found by Glaser et al.
2. Chemical constitution of the Iron.
3. Dimensions of the Search Coils.
4. The Effective Induction $\overline{B}$ for various points over the useful area.
5. The effect of Momentum Loss on Particle Displacements.
6. The accuracy of the approximate treatment of Momentum Loss.
7. The Median Momentum for each Category.
8. The Particle Rate for each Category.
9. The Day-Night Particle Rate from each Category.

CHAPTER 1.

General Introduction

The general picture of the Cosmic Radiation, considering such aspects as the nature of the primary radiation and the mechanism of its interaction with the nuclei at the top of the atmosphere, is now moderately well understood, although the origin of this radiation remains at present the subject of conflicting postulate and theory.

The primary radiation incident on the top of the atmosphere from outer space constitutes a flux, or stream, of atomic nuclei of various energies up to at least 10^{18}eV, almost isotropic in space and remarkably constant in time. It is composed predominantly of protons (~85%), the remainder being α-particles and heavier nuclei. The protons are absorbed exponentially with an absorption length of about 120 gm cm^{-2} and thus the protons may be considered to interact with the Oxygen and Nitrogen nuclei of the atmosphere mainly within the first 200 gm cm^{-2} pressure band and, in the case of the α-particles and heavier nuclei, which have shorter absorption lengths, at higher levels. In consequence most of the Cosmic Radiation interacts with the atmosphere above 50,000 ft. from sea level. The interactions give rise to secondary radiation consisting of charged (both positive and negative) and neutral π-mesons, heavier mesons and hyperons. These secondary particles produce further mesons and nucleons by inelastic collisions with air nuclei, and also electrons and photons by a variety of processes.

The charged π-mesons have a mass of 273 times that of the electron and a mean life of 2.6×10^{-8} sec and either decay in flight into μ-mesons and neutrinos, or interact with nuclei and undergo inelastic collisions. The μ-mesons, particles of mass 207 times that of the electron, are weakly interacting particles and have the comparatively long lifetime of 2.2×10^{-6} sec. This long lifetime enables many of them to reach sea-level and the more energetic of them penetrate to great depths under the ground. They therefore form the predominant part of the so-called hard or penetrating component.

The neutral π-meson has a mass of 264 times that of the electron, a mean life of about 10^{-16} sec and decays into two photons. These photons initiate cascade showers of electrons and photons to form an important part of the soft component of the radiation at sea-level.

Many studies have been made of the variations of the components of the cosmic ray flux with respect to time and direction. Such variations are important for a variety of reasons, and these can best be appreciated by considering the life history of the cosmic ray particles from their creation in outer space to their detection or the detection of their progeny in the laboratory.

It seems likely that a fraction, at any rate, of the cosmic radiation is produced in the envelopes of super-novae and other very hot stars. Then on its passage to the earth the radiation interacts with the galactic material and is acted upon successively by the galactic magnetic field, the sun's magnetic field if any, and the earth's magnetic field. Finally it enters the earth's atmosphere as a high energy primary particle, to initiate the sequence of the events described in the preceding paragraphs, the end product being the sea-level flux; the μ-meson constituting the vast majority of this flux.

In principle, variations of any of the factors entering into the life-history of the cosmic rays; galactic fields etc., will affect the μ-meson flux at sea-level. In practice, however, there are mitigating factors. For example, a μ-meson of average energy at sea-level of say 2 GeV, was probably produced (via π-meson decay) by a primary proton of energy 20 GeV, and the factor under consideration might not affect primaries of as high an energy as this. Variations in the flux of low energy primary particles are obviously best studied at great heights, i.e. balloon or rocket altitudes. On the other hand phenomena associated with high energy primaries can best be studied in laboratories where the operation of apparatus of great size, weight and complexity is possible. For example direct measurements of particle momenta involving iron cored or permanent magnets can be made.

Variations in the secondary cosmic ray flux, arising from changes in the atmospheric parameters - pressure, temperature etc., are obviously best studied in the lower levels of the atmosphere, and many laboratory experiments have been carried out on this topic.

The scope of the present work is the study of flux variations of the μ-meson component at sea-level with reference to time and direction, and their interpretation in terms of contemporary theories of atmospheric variation effects. The studies have been made using a spectrograph comprising a solid iron magnet with arrays of Geiger counters as the detecting elements. This latter instrument has been designed in conjunction with Bennett and Nash (1960) and it represents the only reasonably economical means of obtaining a high uniform magnetic field over a relatively large area, factors which are essential for statistical investigation of the μ-meson flux at sea-level.

CHAPTER 2.

Variations in the Intensity of the μ-meson Component at Sea-Level.

2.1 Historical Introduction.

Exhaustive review papers on the flux variations in general have appeared (Elliot, 1952; Sarabhai and Nerurkar, 1956; Dorman, 1957) and these all show that the largest variations are due to variations in the meteorological parameters. It is these variations that will be discussed here. The existence of a correlation between the intensity of sea-level cosmic rays and meteorological factors appears to have been first pointed out by Myssowsky and Tuwim in 1928. These workers found that a change in barometric pressure of 1 mm Hg produced a change in intensity of 3.45%, the changes being in opposite directions. This variation was correctly interpreted as being due to the increased absorption and therefore lower intensity at higher atmospheric pressure and vica versa at lower pressure.

With the development of cosmic ray detectors having high counting rates and improvements in the collection of meteorological data, particularly regular measurements of upper atmosphere data with balloons, further correlations became apparent.

2.2 The Equation of Duperier.

These correlations can be most conveniently understood from the early work of Duperier (1949). Duperier showed, by analysis of the day to day changes in the intensity at sea-level, that the changes could be correlated with the following meteorological factors.

1. The barometric pressure - P.
2. The height of the 100 mb level in the atmosphere - H.
3. The average temperature of the atmosphere between the 100 mb and 200 mb levels - T.

Thus, considering the fractional change in intensity I/I at sea-level and the parameters P, H and T, they may be related by the following equation.

$$\frac{\Delta I}{I} = \alpha_P \Delta P + \alpha_H \Delta H + \alpha_T \Delta T$$

where P, H and T represent the changes in the respective parameters, the α's being their respective coefficients.

Considering the physical significance of the various parameters it can be seen that α_P represents the mass absorption effect; an increase in pressure will cause more low energy μ-mesons to be absorbed by the atmosphere before they reach sea-level with the corresponding decrease in intensity. α_H represents the decay coefficient, and may be interpreted as the change in survival probability arising from a change in height of the meson formation; an increase in H causes more μ-mesons to decay into electrons before reaching sea-level, thus again the intensity falls. The third parameter, α_T, is the positive temperature coefficient due to the competition between π-μ decay and nuclear capture of the parent π-meson near the production level; a rise in temperature gives a corresponding fall in density and consequently more π-mesons decay and fewer interact since the average interaction distance will increase. At sea-level this will result in an increase in intensity of μ-mesons with increasing temperature of the upper atmosphere.

2.3 More accurate analyses of the Meteorological Effects.

Many over-simplifications of physical processes involved have been made in deriving the regression formula; for example, μ-mesons are not in fact generated at a unique height but have a probability of generation which varies with height, T and P are not independent etc. In practice therefore it is found that the coefficients are not strictly constant but vary with time, for each experimental arrangement and inconsistencies appear between the results from different arrangements. In particular widely differing values of α_T have been found by different workers, ranging from -0.023 ± 0.027 to +0.123 ± 0.024% per ^{o}C (Bachelet and Conforto (1956) have summarized the discrepancies). Much more elaborate regression formulae have in consequence been developed to take account of these factors, demanding a knowledge of the physical conditions over the whole of the atmosphere and not only at a few selected points. These treatments have been carried out by a number of authors notably Olbert (1953, 1955) and Dorman (1957), and have resulted in more satisfactory agreement between theory and experiment (e.g. the results of Matthews, 1959). A more detailed discussion will be given later.

A further important point that can be considered here is that the coefficients in the simple regression formula represent the aggregate effect summed over particles having a wide range of momenta, over the whole of the sea-level momentum spectrum in fact. Now the theoretical analysis, as distinct from the empirical analysis of Duperier (1949), consider the expected variations as a function of momentum. Referring to the simple regression formula we should expect the coefficients to vary with momentum as follows:

1. α_p should fall with increasing momentum since as the momentum rises the amount lost in traversing the atmosphere (2 GeV/c) becomes less and less important.
2. α_H should fall with increasing momentum because at the higher momenta the probability of μ-e decay becomes progressively smaller.
3. α_T should become more important at high momenta since it is only at high momenta (20 GeV/c) where there is significant loss of π-mesons by interaction rather than decay.

2.4 Experimental studies of the Variations as a Function of Momenta.

Systematic experimental studies of the intensity variation as a function of momentum have not been made. Some work has been carried out however. For example, measurements have been carried out using counter telescopes under absorbers so that the data refer to particles having energy greater than some minimum value E_{min}. Thus, measurements were carried out during the International Geophysical Year using counter telescopes at sea-level, with a thin absorber to give E_{min} = 0.4 GeV, and at various depths underground: 25 metres water equivalent (M.W.E.), giving E_{min} = 6.4 GeV and at 55 M.W.E., giving E_{min} = 14.4 GeV. These measurements, Dorman, (1957), have shown that there are no gross discrepancies between experiment and theory but a more detailed experimental study of the momentum (or energy) dependence is still desirable. An attempt to make such a study is described in a later Chapter of this thesis.

2.5 The Experiments of Glaser et al (1950)

Some rather disquieting results on intensity variations which appeared to show a much larger momentum dependence than might be expected, were found by Glaser et al (1950). Using two counter controlled cloud chambers in a magnetic spectrograph these workers obtained 1547 measurable tracks over a range of momentum extending up to 80 GeV/c. The results gave a differential spectrum represented by the form $N(p) = \text{const } p^{-1.9}$. However there appeared an anomalous dip in the momentum distribution at about 3 GeV/c. This decrease has not been substantiated by later workers (e.g. Owen and Wilson, 1955, Ashton et al, 1960) and must be presumed due to either a large fluctuation or some technical imperfection.

Of greater relevance to the present work was the observation of a small diurnal variation which was momentum-dependent; 1 GeV/c particles being favoured during the day, 3 GeV/c and 6 GeV/c particles being favoured at night as shown in Table 1,

TABLE 1.

The Diurnal Variation found by Glaser et al (1950)

Mom. in GeV/c	Particle Excess day - night	Mom. in GeV/c	Particle excess day - night
0.5	-5	5.0	0
1.0	+5	5.5	-2
1.5	+25	6.0	-5
2.0	+15	6.5	-7
2.5	+10	7.0	-5
3.0	-10	7.5	-4
3.5	-15	8.0	-3
4.0	-10	8.5	-2
4.5	+5	9.0	0

Although such a variation seems unlikely its existence cannot be ruled out for the following reason. The overall variation summed over all momenta is very small so that experiments without momentum resolution would not detect the phenomenon; as has already been pointed out no experiments with (differential) momentum resolution have been performed.

One of the purposes of the present experiment was to examine further this diurnal variation.

2.6 The requirements for an Instrument to Study Flux Variations.

Any experiment in which small variations are to be studied requires an apparatus affording a high rate of collection of particles and it was considered that a spectrograph using a solid iron magnet instead of the more conventional air-cored type would prove satisfactory. Sufficiently accurate momentum determination was judged to be feasible using Geiger counters as detecting elements.

No accurate measurements had previously been made with this type of instrument and considerable development of the solid iron magnet was therefore necessary. The next three Chapters describe this work and the properties of the instrument finally adopted.

CHAPTER 3.

Design and Construction of the Solid Iron Magnet

3.1 General Considerations of Design.

The most widely used technique for the determination of the momenta of fast Cosmic Ray particles is that of magnetic deflection, a technique which it was intended to follow in the present case. On account, however, of the low intensity and high momentum of the μ-mesons, (the component of Cosmic Rays under consideration), a magnetic field of high intensity, and covering a large volume, was required. Due to the μ-meson being a weakly interacting particle, the magnetic deflection need not be obtained in an air gap of a magnet, as is the case with a stongly interacting particle, but can be produced inside magnetised material. Thus there is the possibility of using a magnetic circuit devoid of an air gap. The advantages of such a choice of system, namely magnetised iron, are obvious; high uniform fields may be induced over a large volume for very low power of excitation, since the effective vector acting on a particle in a magnetised medium is the magnetic induction B.

Although the probability of a μ-meson suffering a nuclear interaction in such a magnet is negligible, the probability of appreciable Coulomb scattering is high and this factor sets a limit to the accuracy with which the momentum of a single particle may be determined. At constant field, (induction) over a trajectory of length L, the magnetic deflection increases as L, and the root mean square (r.m.s.) angle of scattering as $L^{\frac{1}{2}}$, thus giving a fractional error of a single determination varying as $L^{-\frac{1}{2}}$. An increase in L also increases the maximum detectable momentum, (the momentum corresponding to the smallest deflection to which significance may be attached). Thus, a high value of L appears desirable in every way. However, this reasoning in favour of a high value of L is not true where low momentum particles are to be considered, where the momentum loss in penetrating the iron is important. The minimum momentum required to penetrate the magnet also varies approximately as L. Thus a compromise is required for the length of the trajectory L, i.e. the height of the magnet.

This use of magnetised iron for deflecting Cosmic Ray particles is not new. Rossi (1931) suggested the use of magnetic lenses for the partial separation of positive and negative mesons, and Bernardini et al (1945) used it with success in measurements of the positive excess at Sea Level. These workers used a triple coincidence system with four iron cores, the cores arranged in pairs to act roughly speaking like a cylindrical magnetic lens which concentrates the particles of one sign. Finally Conversi et al (1945) used this system of magnetic lenses to concentrate on an iron absorber alternatively positive and negative mesons, for work on decay processes.

3.2 The Magnetic Material.

The reasoning in the previous section concerning the possibility of using a solid iron magnet assumes that the factors in its favour, namely are intense field of high stability and uniformity covering a large volume, may in fact be obtained. This is not the case without careful consideration of the factors involved, and to this purpose considerable preliminary investigations were carried out on $\frac{1}{10}$ scale models by Bennett and Nash (1960), and Bennett (1960). It was from the results of these investigations that the best compromise was obtained, and the design of the present magnet completed.

The conditions which the magnet was required to satisfy were :-

1. That the useful area, that is the area to be used for the actual deflections of the μ-mesons be large, and that over this area the line integral of the magnet induction should not vary by more than a few per cent.
2. That for low excitation current the $\int BdL$ be stable for small changes in the excitation current.

To satisfy the former condition was a question of geometrical design, to which end the model experiments were carried out; but to satisfy the latter condition was a question of the magnetic properties of the material used. The iron chosen was made to British Standard 24, Part 6, Specification 18, the chemical constitution of which is given in Table II, the relevant portion of its hysterisis loop being shown in Fig. 1. As can be seen from the figure the majority of the portion AB runs almost parallel to the H (field strength) axis, where the iron may be said to be saturated. It was obvious that the magnet should be operated as near to the saturation level as possible, for it is here that condition 2 is satisfied.

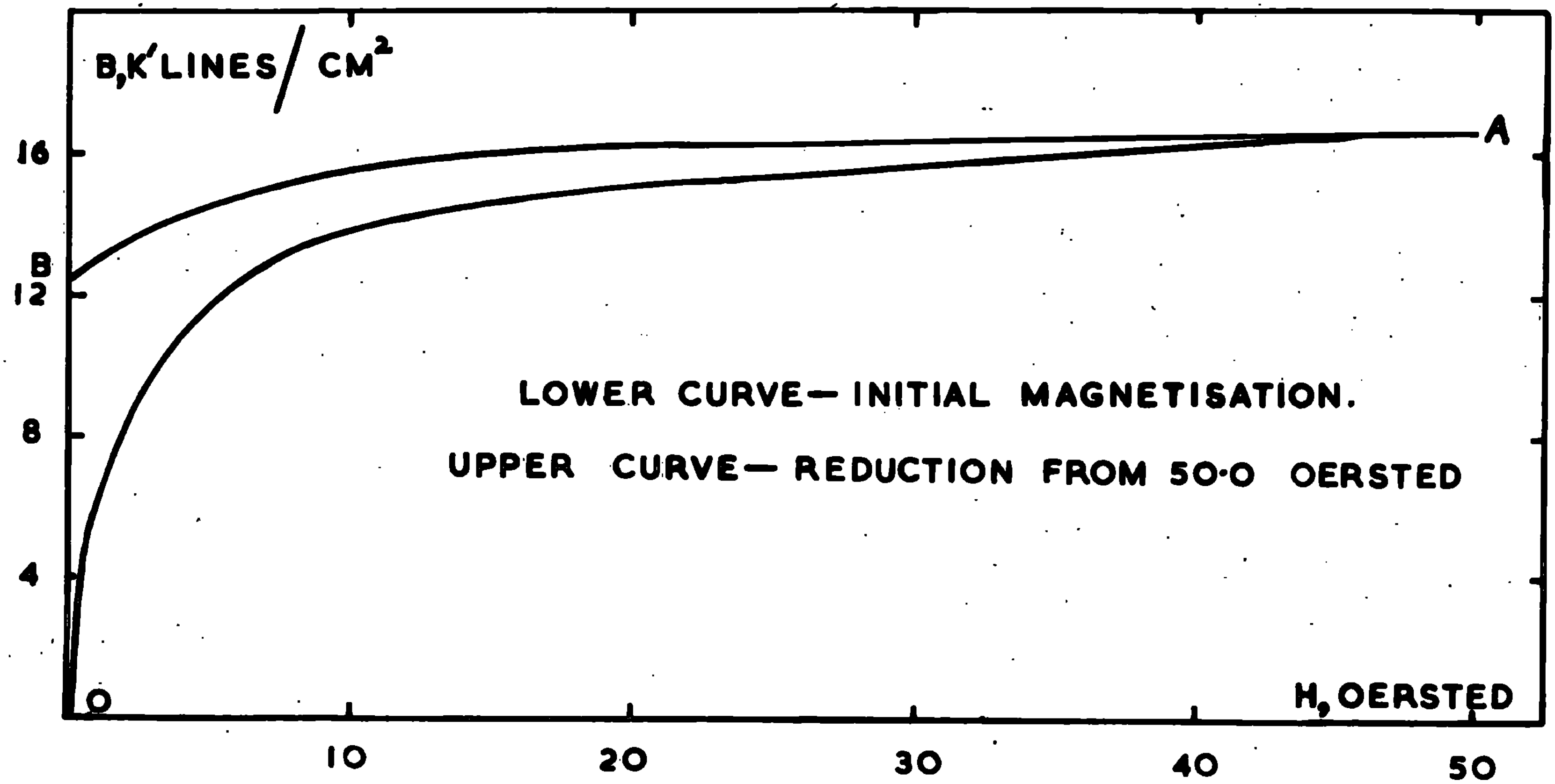

RELEVANT PORTION OF HYSTERISIS LOOP FOR B.S. 24, PART 6. SPEC. 18.

FIG. 1.

TABLE II.

Chemical Constitution of the Iron.

ELEMENT	C	S	P	M_n	S_i	C_r	N_i	C_u	S_n	C_o	A_s	V	A_l	M_o	IRON
% by weight	.07	.026	.01	.36	.01	.021	.11	.20	.026	.017	.031	.01	.038	.015	99.0

3.3 Results of the Model Experiments.

The following is a summary of the work, already mentioned, carried out by Bennett and Nash (1960) and Bennett (1960).

The general form of the magnet originally envisaged is shown in Fig. 2. It was in the form of a 150 cm square, with a 50 cm square hole in the centre, and was thus in the form of a picture-frame. The depth was of the order of 100 cms, made up of $\frac{1}{2}$" steel plates. Rectangular variations on the above pattern were also considered, and it was with these dimensions in mind that the $\frac{1}{10}$th scale models were constructed.

The prime factors considered by Bennet and Nash were the variation of magnetic flux B over the whole of the picture-frame (i.e. in the X and Y direction as shown in the figure) and also the variation in flux down through the magnet (i.e. in the Z direction). Also considered was the variation of the line integral $\int BdL$ over the magnet, including also the leakage flux, and the variation of the flux density with time. Finally various models were constructed to observe the effect of rounding-off either the inside or outside corners.

GENERAL DESIGN OF THE MAGNET

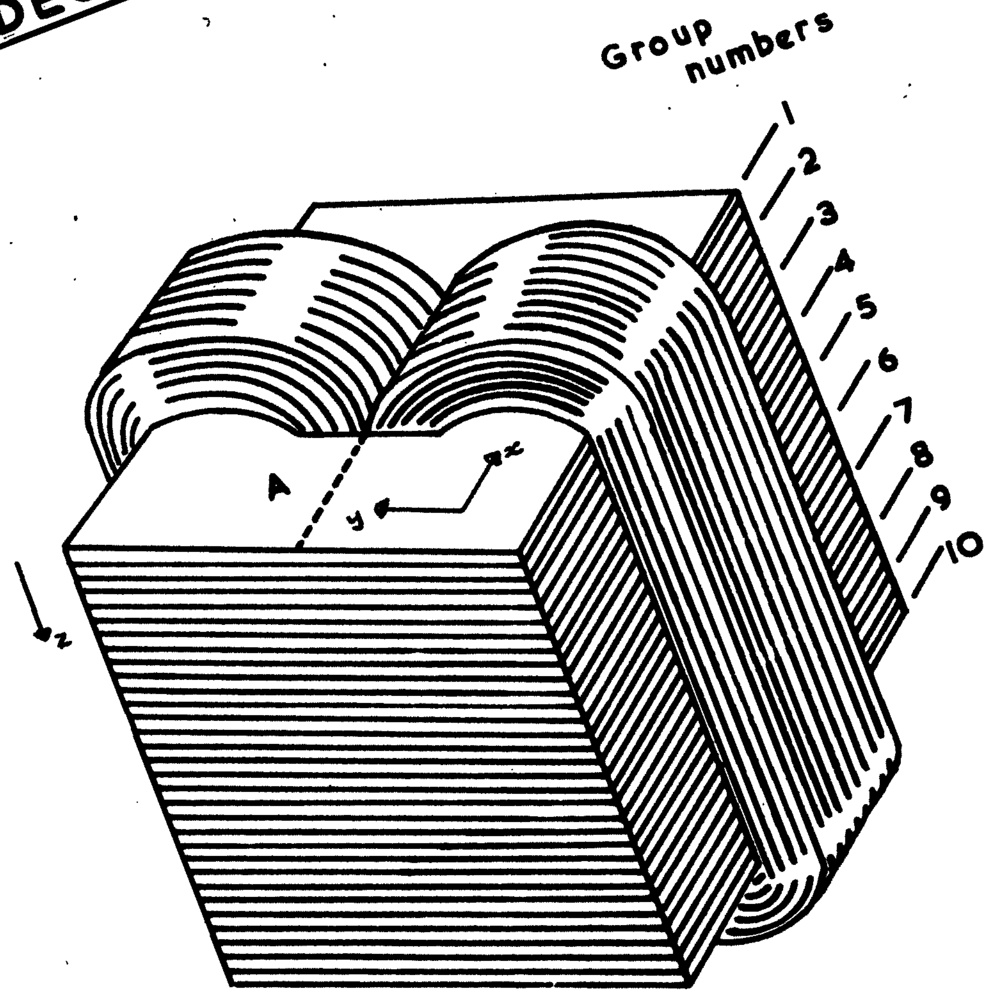

FIG 2.

The results obtained may be summarised as follows.

1. Either the region covered by the exciting coils or the open sides (or both) can be used as deflecting volumes. The advantage of the higher induction under the coils is offset to some degree by the greater degree of uniformity in the open side, and the ease with which induction measurements can be made.
2. Although the radius of curvature of the outside corners appears to have a negligible effect, the radius of the inside corners is of considerable importance if the useful region is to approach these corners.
3. Even at comparatively low degrees of excitation the variation of $\int Bdl$ over most of the selected side is not large.
4. Increase in the flux density, produced by a large increase in magnetising current for a short period, is stable, decay integrated to infinite time giving a total decrease of only 0.03%.

3.4 Design and Construction of the full-scale Magnet.

The results and conclusions of the model experiments gave some idea of the performance to be expected from typical designs. The design chosen was in practice a compromise of a number of factors, the most important being.

1. The rate of collection of particles.
2. The line integral of magnetic induction $\int Bdl$.
3. The signal to noise ratio for individual particle deflections i.e. the ratio of the deflection of the particle produced by the magnetif field to the r.m.s. deflection of the particle produced by Coulomb scattering.

A high value for this last factor was not considered necessary, since the experiments to be carried out concern the measurements of momentum spectra, and the effect of scattering can be allowed for when a large number of trajectories are considered. The compromise dimension of 25" was chosen, for which the signal to noise ratio was 3.74, at an excitation current of 16 amps. The magnetic deflection is then 1.68° for a particle of momentum 10 GeV/c, the magnetic induction produced in the iron by the excitation current being of the order of 15.5 K. Gauss. With this height the momentum loss in penetrating the iron is 0.89 GeV/c.

It was from the point of view of ease of assembly that the magnet had been envisaged as constructed from $\frac{1}{2}$" 'boiler plate'. The model was manufactured from $\frac{1}{2}$" plate. Experiments showed no disadvantages of this laminated construction and the actual magnet was in fact fabricated from boiler-plate of the above nominal thickness. The magnet consisted of 50 'laminations', each weighing 4.2 cwt, mounted horizontally and held in place by vertical steel pegs through two diametrically opposite corners. The general arrangements are shown in Fig. 3(a). The sides B and C were used for the deflection of the μ-mesons, side C is shown in detail in Fig. 3(b).

Provision for the measurement of the magnetic flux within the magnet itself was made by the insertions of insulated wires between every group of 5 plates. In addition to this, wires were inserted between successive plates in the top most-but-one group C_2.

3.5 <u>The Excitation of the Magnet</u>.

The excitation energy was provided by coils of 14 S.W.G. double cotton covered copper wire wound on to the sides B and C as shown in Fig. 3(a). Each coil consisted of 250 turns, the total resistance being 7.2 Ω

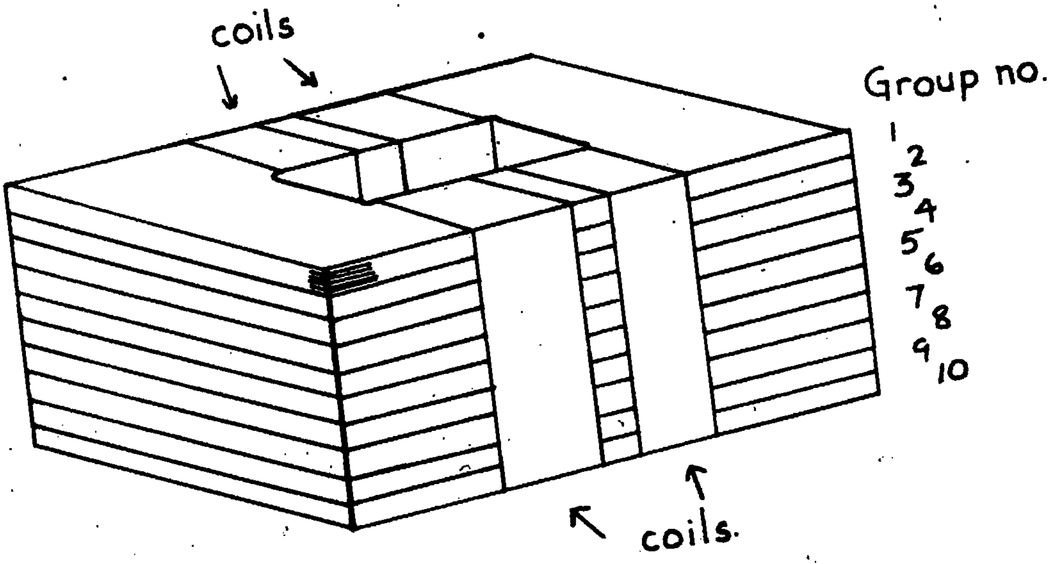

FIG. 3a

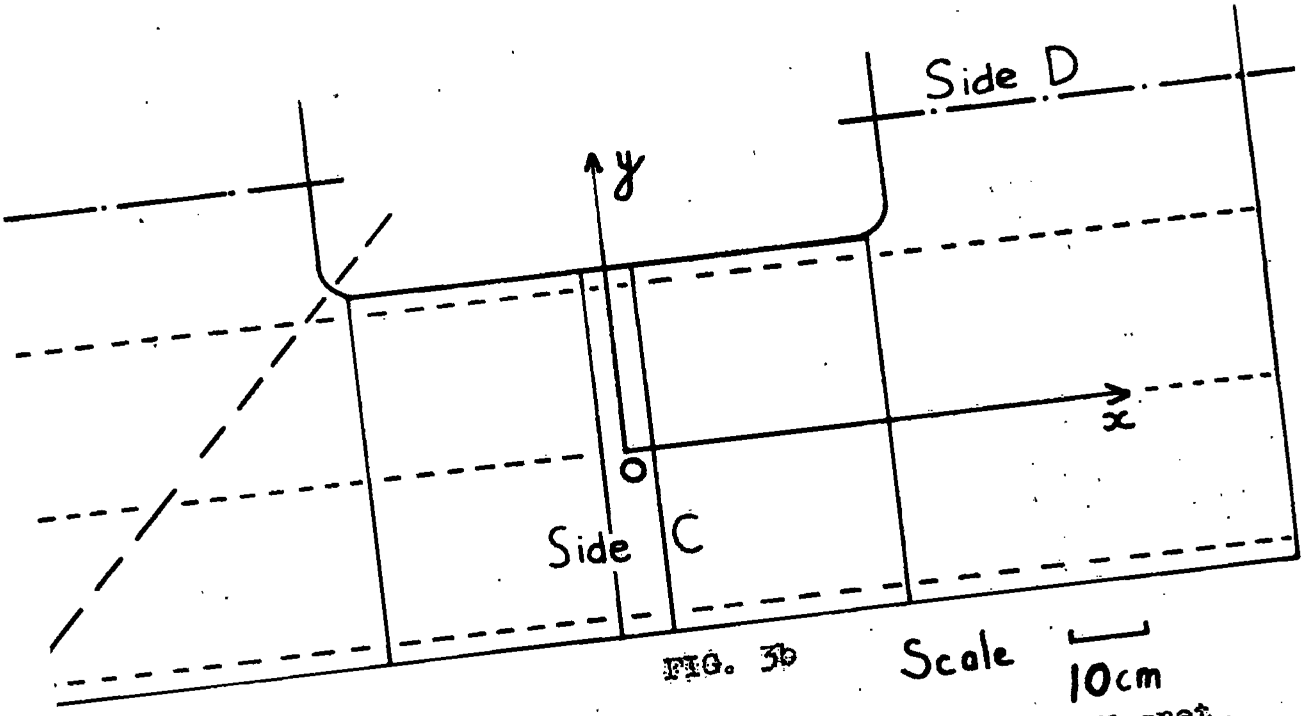

FIG. 3b

FIG. 3 Finalised design of the Solid Iron Magnet when cold and the self inductance being 210mH (at $1kH_z$). The actual energy of excitation was provided from the A.C. mains by means of an ex G.P.O. copper-oxide rectifier, which provided a D.C. potential of 125 volts giving a maximum excitation current of 18 amps. Natural convection provided sufficient cooling for both magnet and rectifier, provided the excitation current did not exceed 20 amps, at which it was tested using an extra subsidiary supply. At 16 amps, the normal working current, the power dissipated was 2 K.W, the temperature of the magnetic coils 50°C, and the magnet iron 28°C, for an ambient temperature of 19°C.

3.6 Later Modifications for Measurements on Horizontal Cosmic Rays.

Although the later experiments to study the flux of cosmic rays at large zenith angles are not described in this thesis a description of the modifications to the magnet is useful and will be given here. In order to use the magnet to obtain data on the horizontal flux, it became necessary to design a new framework, to mount the 50 laminations rigidly in a vertical plane. The new framework used in this case is shown in Fig. 4. Here the plates are held in place by 4 Hexagonal Whitworth $\frac{3}{4}$"

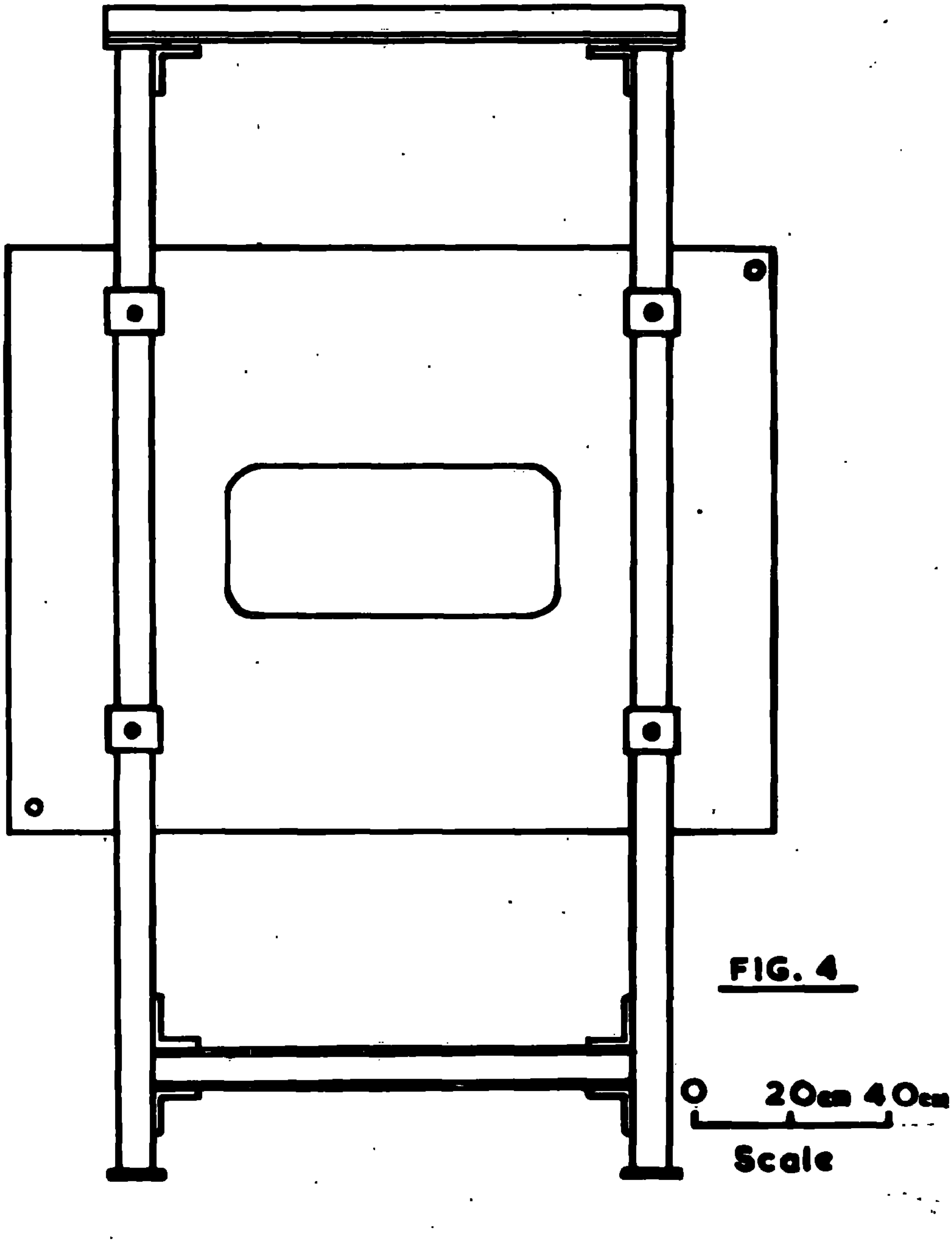

FIG. 4

REDESIGNED FRAMEWORK FOR HORIZONTAL EXPERIMENT.

bolts as shown, the steel pegs now being used merely to align the plates.

Opportunity afforded by the re-mounting of the magnet, was taken to increase the number of turns on each coil on sides B and C. from 250 to 275, making a total of 550, an increase of 10%. The total resistance of the circuit when cold was now raised from 7.2 Ω to 7.95 , and the self inductance to 230mH(at 1 KH$_z$). With this increase in resistance it was still possible to obtain the normal working current of 16 amps, and thus the extra turns were used in an attempt to lessen still further the dependence of the line integral $\int Bdl$ on the excitation current, and to produce greater uniformity of magnetic flux over the useful area.

CHAPTER 4.

Measurements on the Magnet.

4.1 The Parameters under Investigation.

A basic requirement of a magnet is constancy of flux against variations of various parameters. In the Spectrograph for which the magnet was designed the particles are deflected in the core, and to a lesser extent in the air above and below the core and it was therefore necessary to measure the magnetic flux distribution in these regions for a wide range of experimental conditions.

In principle it was necessary to determine the line integral of the magnet induction in the direction Ox for many trajectories distributed throughout the useful volume of the magnet. Considering side C (Fig. 3b) it was hoped that the useful volume would be only a little less than the volume contained by the coils on that side, edge effects being the limiting factors. Here, it was hoped that there had been reduced to a minimum by the actual design, especially the rounding of the inside corners. It was comparatively easy to measure the line integral $\int H_x dZ$ arising from the leakage flux above and below the magnet, but measurement of the flux within the magnet presented difficulties.

It was here that consideration was given to the use of a magnetic potentiometer. A modern form of this instrument was described by Margerson and Sucksmith (1946), who indicated that the instrument must be small if it was to measure variations of H over a small area. The instrument, which is in the form of a semi-circular coil, measures the magnetic potential difference $\int H dl$ between its feet.

After a careful consideration of the instrument, an attempt was made to construct one, but this proved exceedingly difficult as the coil had to be very carefully and evenly wound with fine guage wire onto a semi-circular former. It was therefore considered that as the accuracy of the instrument depended to a great degree on the accuracy of its construction, and as indeed little seemed to be understood about the actual physical conditions under which the instrument worked, it would be impossible without extensive study of the actual instrument itself to obtain anything more than a rough estimate of the flux in any-one position, and it was dispensed with.

The measurements that were made directly, using the standard technique of determining the flux through a coil, with a fluxmeter, were $\int B_x dA$ over each group at the centre of each side, $\int B_x dA$ over each plate within group C_2, at the centre of side C, and the variation of $\int_{\Sigma n} B_x dA$ over the whole side as a function of x. An important quantity, not measurable by this technique, was the variation of B_x with y, and this could only be inferred by comparison with the results of the model experiments.

Consideration was given to reasons for non-uniformity of B. These could be devided into two classes.

1. The geometry of the system.
2. Variation of magnetic properties from plate to plate within the magnet, or even variation of magnetic properties within a single plate.

In the case of class 1, the main variation would be the change of B_x with y arising from the gradient of magnetising field within the coils; Bennett and Nash showed that the variation of $\int_x B_x dZ$ with y was ± 2% over the useful area, and this result was considered applicable to the full size magnet.

In the case of class 2, measurements on the full size magnet were necessary. Variations over one plate were expected to be small, but some measurable change from plate to plate was expected, and the measurement of $\int B_x dA$ enabled this to be studied. In practice this variation was not very important as the deflection, and displacement, of particle trajectories could be calibrated, if the form of the variation was accurately known.

Finally an extensive study was undertaken of the leakage flux above and below the magnet. This was useful for two reasons; firstly it gave the contribution to $\int H_x dZ$, and secondly it provided some information on the direction of the lines of force within the magnet.

4.2 The Fluxmeter.

All the flux measurements were made using a calibrated Grassot Fluxmeter, the form of the instrument used being described by Hickstall-Smith (1932). As the full scale deflection of the instrument was only 4.5×10^5 Maxwell-turns, it was necessary to extend the range by means of non-inductive shunts. On open circuit the period of the instrument was about 50 seconds. For measurement of induction in the iron the excitation current in the coils was reversed twice, positive to negative and vica versa, and the mean of the two deflections taken. For the leakage flux measurements search coils were reversed in a steady field. For comparison three coils were used, their dimensions being given in the table below.

TABLE III

Dimensions of Search Coils.

	No. of turns	Diameter of Coil (cm)	NA
Coil A	100	3.8	1310
Coil B	125	2.9	785
Coil C	400	2.2	1385

4.3 Variation of Magnetic Flux with Time.

This variation is the product of two variations, physically independent. They are

1. Variation of magnetic flux with excitation current.
2. Variation of excitation current with time.

The total flux was measured as a function of excitation current over the range 12-17 amps using as search coil a single turn wrapped round the whole side. The mean induction was then derived from a knowledge of the mean thickness of the plates (0.507" - see § 4.4 for details of the determination of this mean) and the data are presented in Fig. 5, the diameters of the circles representing the errors. These arise mainly from the lack of complete reproducibility of the fluxmeter deflections.

Useful quantities can be derived from this graph. Thus, at a mean current of 15 amps, the variation of induction with current is

$$\frac{\partial B}{B \partial I} = 1.19\% \text{ amp}^{-1}$$

A more useful quantity is the fractional change of induction to that of current

$$\frac{I \partial B}{B \partial I} = 0.178$$

This figure compares favourably with the value of 0.1 found in the model experiments.

To observe the second variation i.e. the variation with time, and to check that it remained within the limits permissible, a (shunted) recording milliammeter was included in the magnet current circuit. In this way a continuous record was obtained of the excitation current over the whole period of operation of the

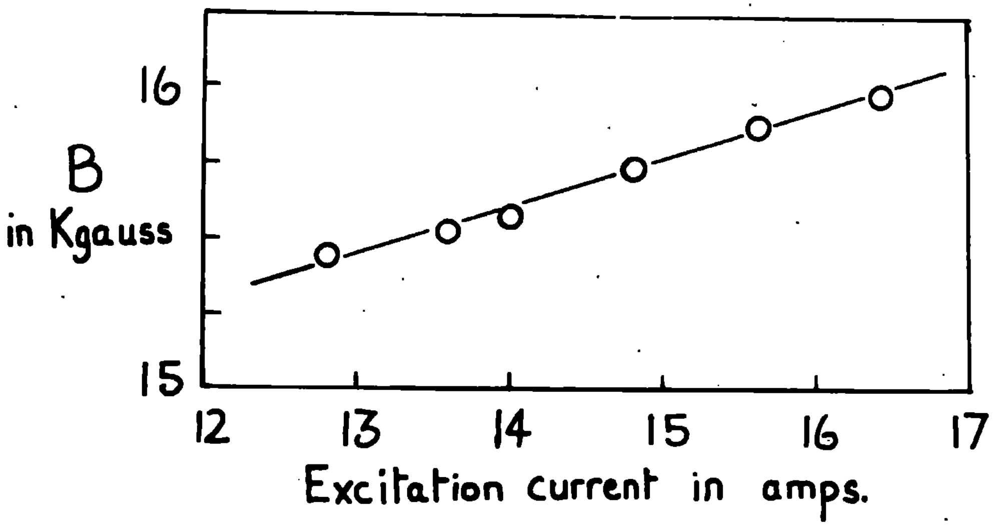

FIG. 5 Variation of Magnetic Flux in the Magnet with Excitation Current.

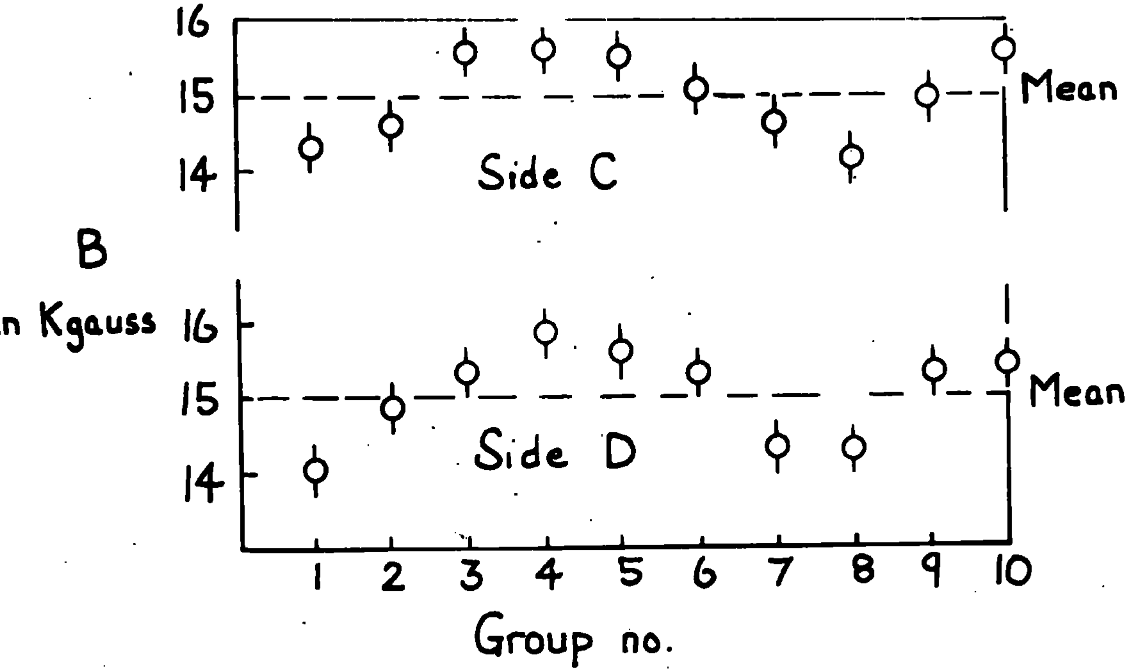

FIG. 6 Variation of Magnetic Flux in the Magnet with Group Number.

apparatus. The current variations arise from a variety of factors mainly mains voltage variation and ageing of the rectifier.

To obtain an estimate of the variation a period of 28 days continuous recording was analysed and a histogram was plotted of the current at 15 minute intervals. The histogram was found to be close to a Gaussian distribution with a standard deviation of ± 1.3%.

$$\text{i.e. } \left.\frac{\partial I}{I}\right._{\text{R.M.S.}} = 0.013.$$

It is possible to obtain an estimate of the total variation of flux with time over the period concerned from a combination of the two factors discussed. Thus

$$\left.\frac{\partial B}{B}\right._{\text{R.M.S.}} = \frac{I\partial B}{B\partial I}\cdot\left.\frac{\partial I}{I}\right._{\text{R.M.S.}} = 0.0023$$

$$\text{i.e. } 0.23\%.$$

This degree of stability was considered to be quite satisfactory.

4.4 Variation of Magnetic Flux with Group Number.

Measurements were made at an excitation current of 15 amps for each group on side C, and side D. An estimate of the mean thickness of the plates was derived by a detailed study of the thickness of the top plate, involving 20 estimations, 5 from each side, and the measurement of the thickness on side C of each of the top 10 plates. Using the mean thickness so derived the results shown in Fig. 6 were calculated. It was immediately obvious that there was a significant variation in induction of similar magnitude for both sides C and D.

It is possible that the variation of thickness both over one plate and from plate to plate, together with the statistical error given to each reading in the figure has been underestimated, but a study of the parameters does not support this view. The error in the estimation of any one plate was found to be less than ± 2%, and the error on each estimation of flux not greater than ± 1%, whereas the variation from the mean for the flux through C_1 was greater than 5%, for C_5 greater than 3%.

The measurement of the actual effect of the variation of plate thickness within the group was therefore undertaken by means of measurements of the flux within each single plate for group C_2. The actual thickness of these plates had already been obtained, and it was thus possible to obtain the true total flux within the plate for a mean thickness of 0.507"; this is shown in

Fig. 7. Here the errors are considerably smaller than in Fig. 6, the thickness of the plate being measured to ± 1%, and the flux to ± 0.3%; clearly the variation cannot have been caused by plate thickness.

For a final check, the measurement of the flux for each group number was repeated for the whole of side C, but this time the excitation current was increased to 18 amps. This showed the same sinusoidal variation, with a higher mean flux, the variation being less pronounced. This tended to suggest a variation in composition, and removed the possibility of the effect being due to plate thickness variation, since if the latter was the case, the variation would remain unaltered even though the mean flux had increased.

The measurements on the scale model showed similar rather large variations but without any sinusoidal aspect. The authors explained it as being due to variation in composition of their plates, in agreement with the conclusions of the present author. The one disquieting feature is the fact that the variations found in the full-scale magnet are sinusoidal despite the random stacking of the plates. It must be concluded that the sinusoidal form is purely by chance.

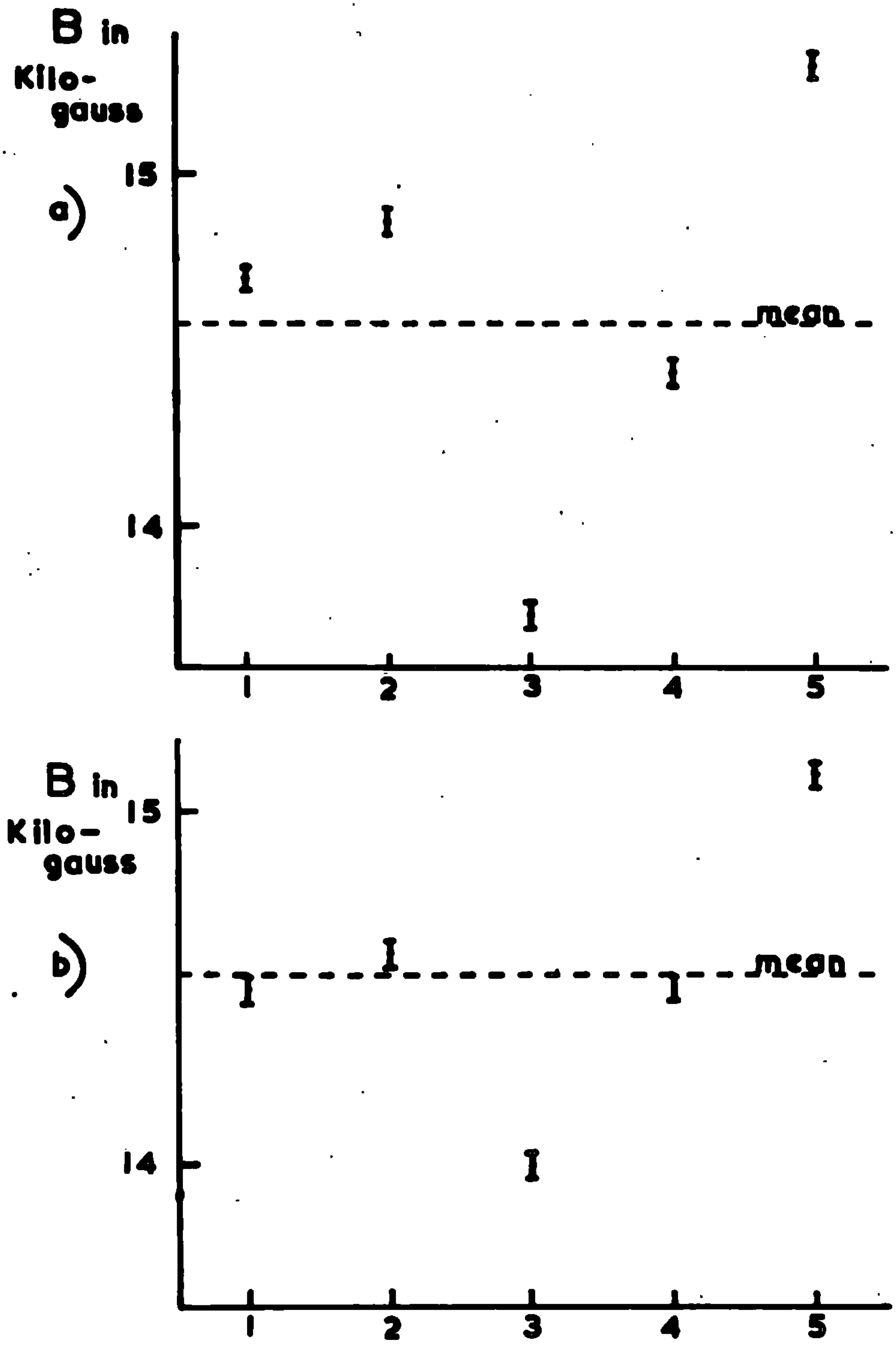

THE MEAN INDUCTION AS A FUNCTION OF PLATE NUMBER OF GROUP C2

a) CALCULATED FROM MEAN PLATE THICKNESS

b) CALCULATED FROM MEASURED PLATE THICKNESS

FIG. 7

4.5 Variation of Magnetic Flux along the OX Axis.

A reduction in flux along the OX axis (Fig. 2b) with increasing distance from the centre of the side may be expected, on account of the increased leakage, which occurs mainly from the inside edge. The results of measurements made with a search coil comprising a single loop round the entire side are shown in Fig. 8. As before, the induction B was derived using the mean value for the plate thickness. The maximum variation of B was found to be ± 1.4%, and therefore was not very important.

4.6 The Measurement of the Leakage Flux.

The results of these measurements may be divided into three groups.

4.6.a. Variation of leakage flux with height.

Measurements were made of the leakage flux in the three mutually perpendicular directions described in the previous Chapter (section 3.3), at points on various axes and at different heights. The variation of H_Z with height above the magnet is shown in Fig. 9 (a and b), the points through which the vertical axes were drawn being shown in Fig. 3(b). The variation of $H_x dZ$ with distance from the OY axis is shown in Fig. 10. (in the

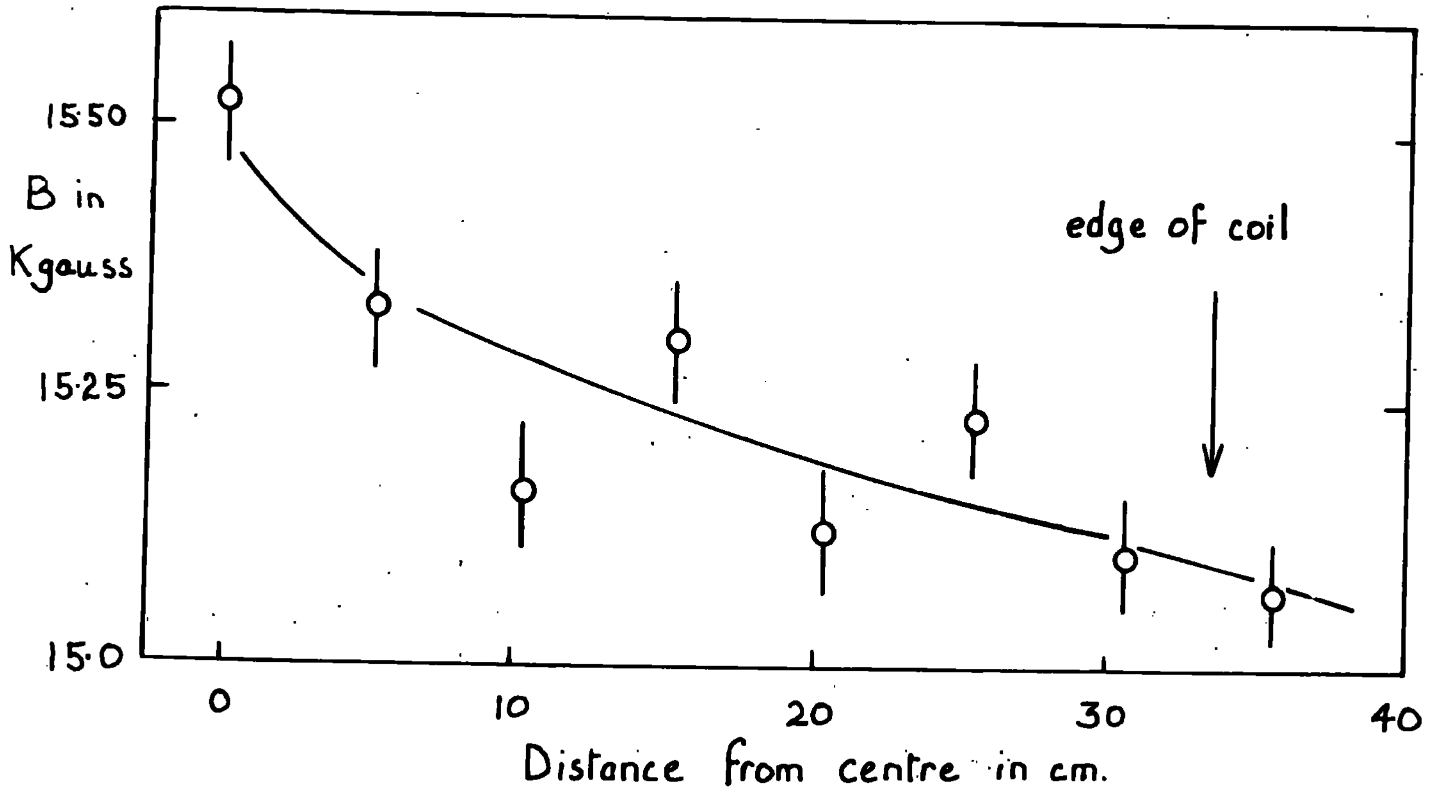

FIG. 8 Variation of Magnetic Flux along the OX axis of the magnet.

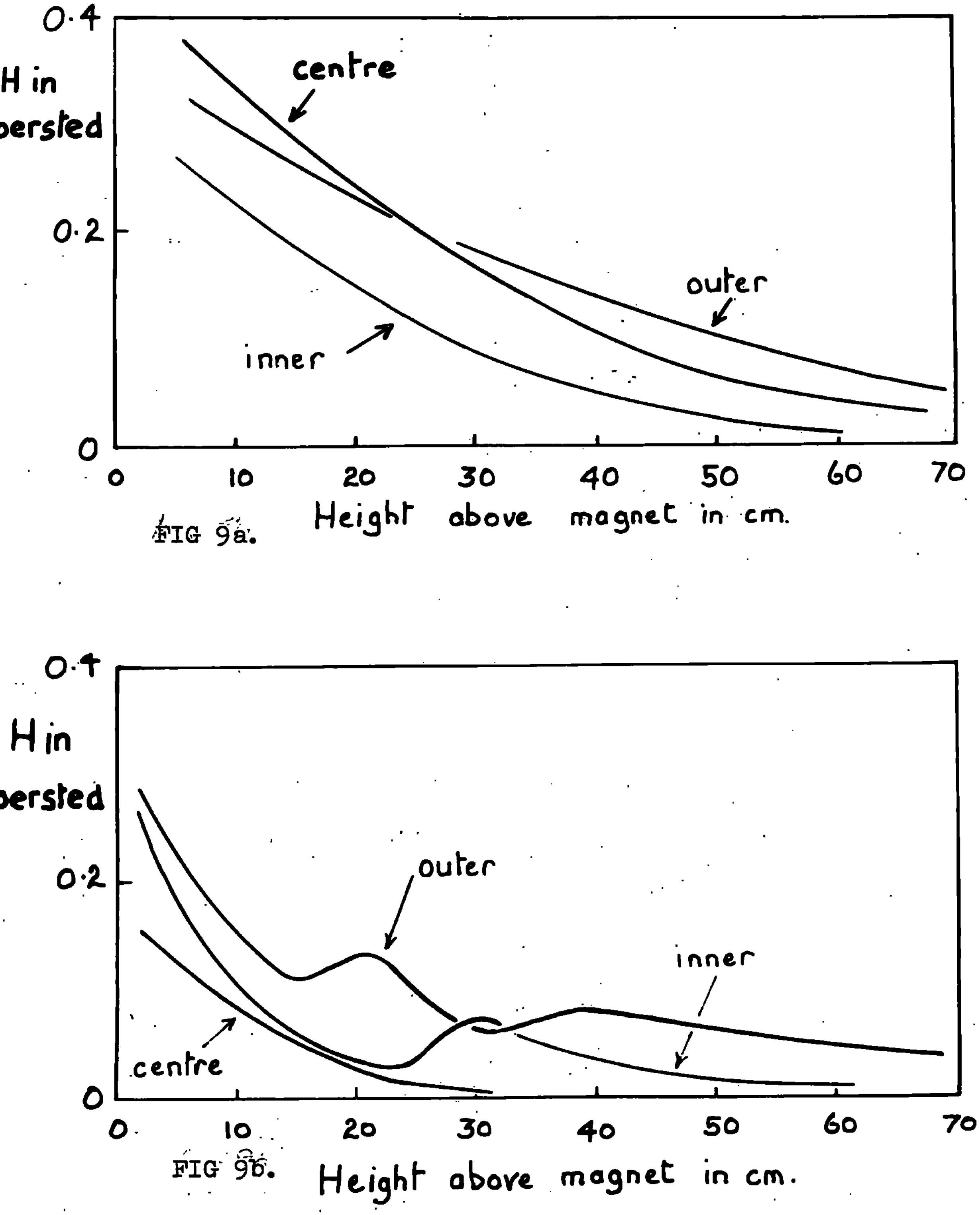

FIG 9a.

FIG 9b.

FIG. 9 Variation of leakage flux with height above the magnet.

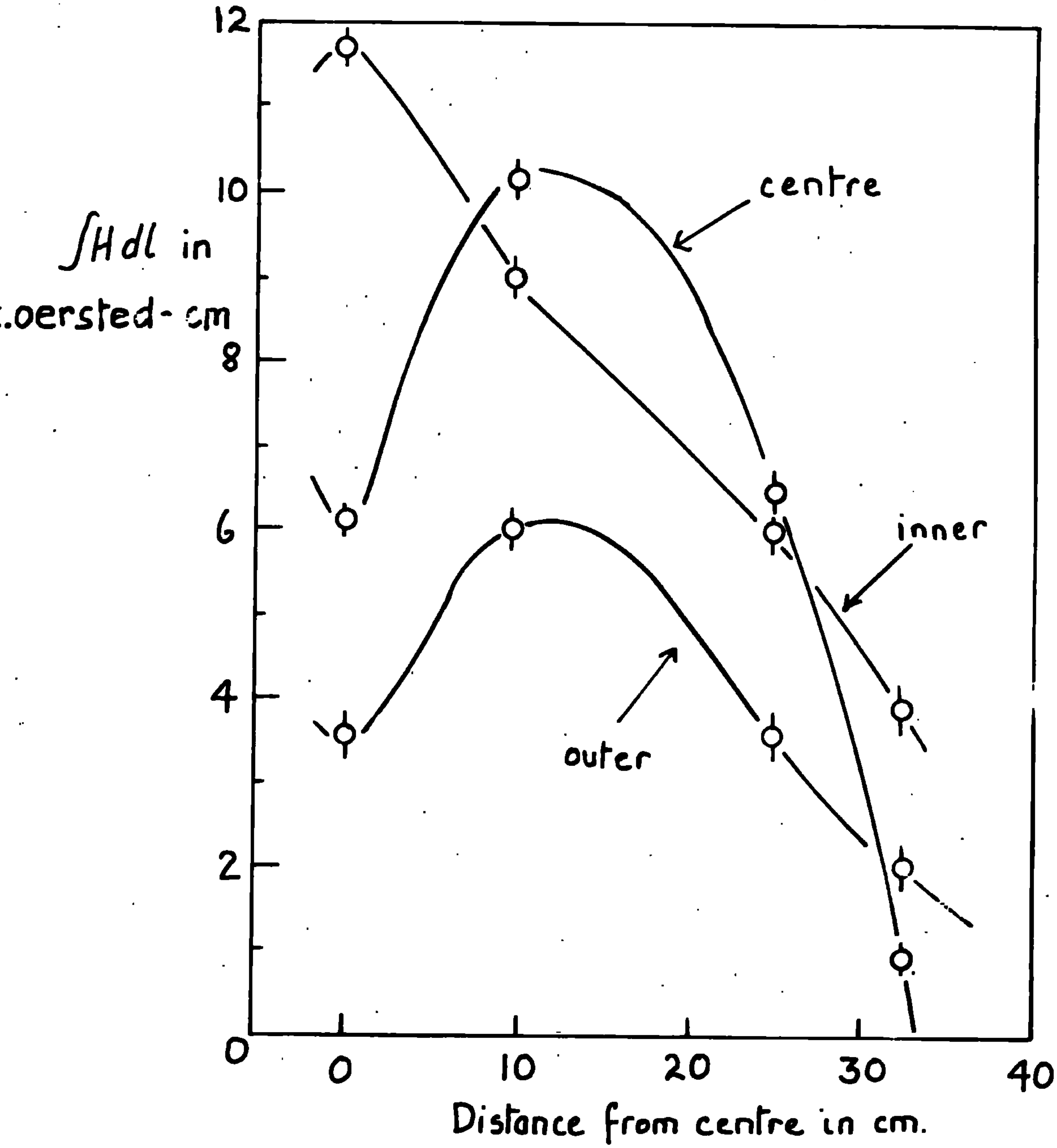

FIG. 10 Variation of leakage flux over the useful area of the magnet.

figure $H_x dZ$ is written as Hdl). The average contribution to the line integral of the field was approximately 2. 6 K. G.-cm compared with a mean value of $\int B_x dZ$ = 960 K G.cm for the same excitation of 16 amps. The fraction was therefore 1.25%, the direction of the leakage field being opposite to that of the induction in the iron.

4.6.b. Variation of integral field strength over the useful area of the magnet.

Considering the variation of the mean value of $\int B_x dZ$ over the width of the magnet, that is, in the OY direction, with distance along OX, its effect was to compensate to some extent for the fall off in induction in the iron for distances greater than 15 cm from the centre. The net result of the variation was to give extreme limits from the mean $\int H_x dx$ of ± 1.7%.

A useful way of presenting the data is to give the effective induction $\bar{B}$ which is that uniform induction which, acting over the height of the magnet, L, would give the same magnetic deflection. Thus $\bar{B}$ is given by the relation

$$B \quad L = \int B_x dZ + \int H_x dZ$$

Values of B have been evaluated for various points on the useful area of the magnet (Fig. 12) and the results are given in Table IV. The excitation for these results was 16 amps.

These results show that the maximum variation from the mean is ± 2.7%.

4.6.c. The Direction of the magnetic induction inside the magnet.

A knowledge of the directions of lines of force within the magnet is sueful for two reasons; it enables a check to be made on the induction measurements and it is also necessary for very accurate measurement of particle deflections.

As mentioned before, a direct determination of the directions was not possible, but some idea could be found from leakage measurements just above the top plate. Near the coils the measurements were unfortunately profoundly modified by the effects of the coils themselves, and an attempt to obtain information on the flux beneath did not produce any satisfactory result. This was not surprising, since as study of Fig. 10 showing the variation along the OX axis, showed quite plainly the effect of a small gap between the coils on that side.

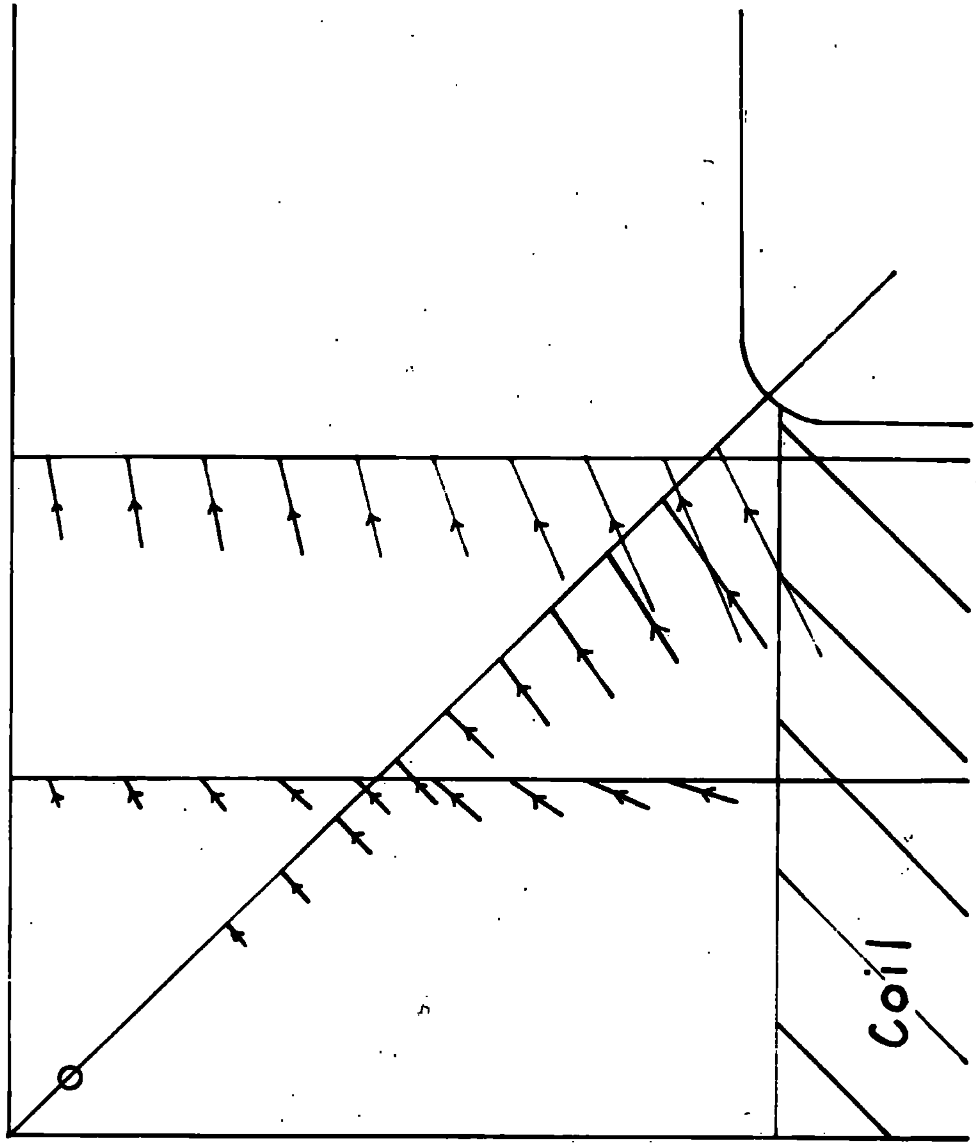

FIG. 1 Vector diagram of horizontal component of leakage flux on surface of magnet.

VARIATION OF TOTAL FLUX OVER USEFUL AREA OF MAGNET.

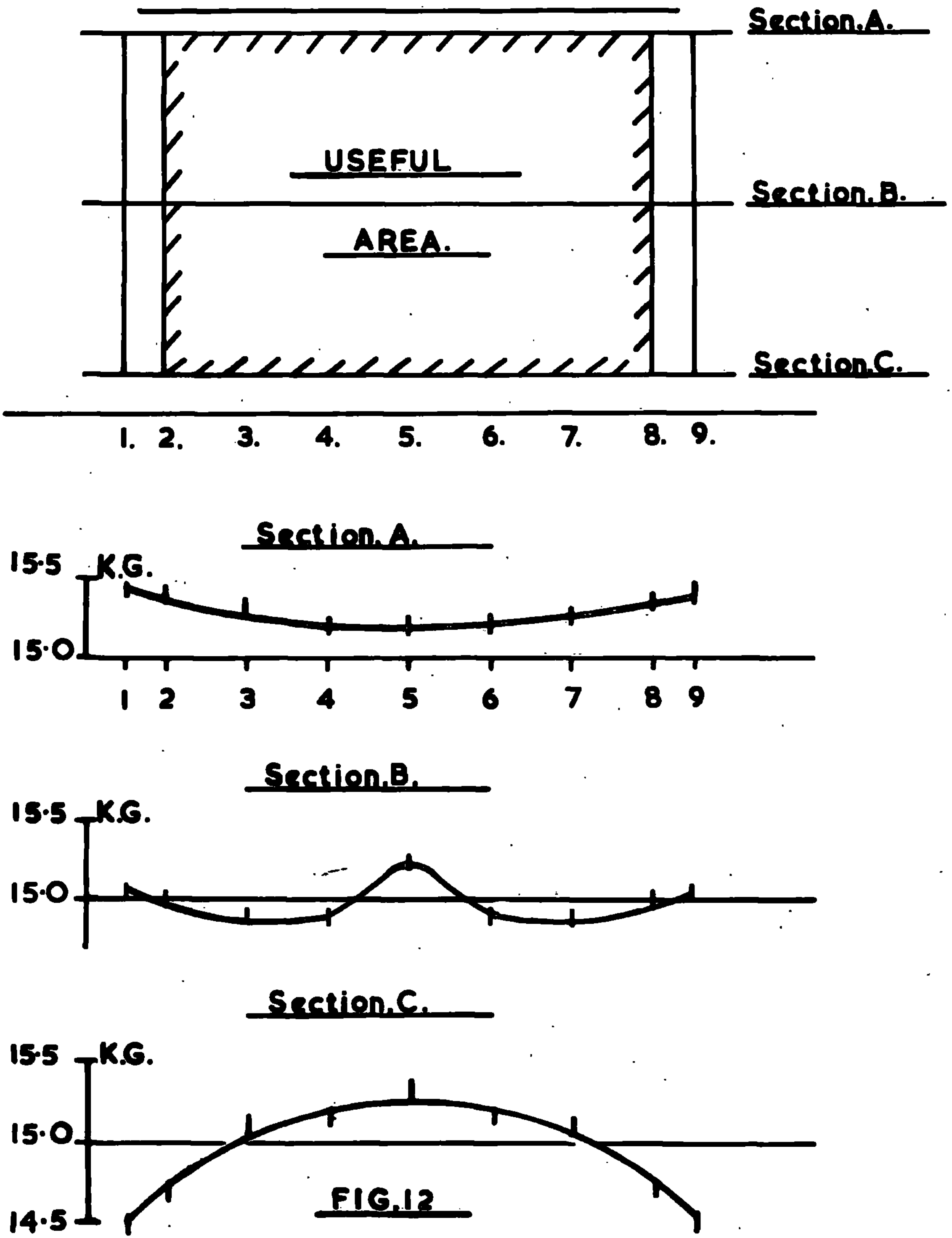

FIG.12

TABLE IV

The Effective Induction $\bar{B}$ for various points over the useful area

	Position (see Fig. 12)	1.	2.	3.	4.	5.	6.	7.	8.	9.
SECTION A	$\int \frac{BdZ}{L}$ in iron	15.50	15.50	15.50	15.50	15.55	15.50	15.50	15.50	15.50
	$\int \frac{HdZ}{L}$ in air	0.10	0.13	0.22	0.29	0.38	0.24	0.22	0.13	0.10
	$\bar{B}$	15.40	15.37	15.28	15.21	15.17	15.21	15.28	15.37	15.40
SECTION B	$\int \frac{BdZ}{L}$ in iron	15.06	15.08	15.17	15.22	15.50	15.22	15.17	15.08	15.06
	$\int \frac{HdZ}{L}$ in air	-	0.06	0.26	0.32	0.19	0.32	0.26	0.06	-
	$\bar{B}$	15.06	15.02	14.91	14.90	15.31	14.90	14.91	15.02	15.06
SECTION C	$\int \frac{BdZ}{L}$ in iron	14.50	14.76	15.20	15.30	15.45	15.30	15.20	14.76	14.50
	$\int \frac{HdZ}{L}$ in air	0.03	0.06	0.13	0.19	0.20	0.19	0.13	0.06	0.03
	$\bar{B}$	14.47	14.70	15.07	15.11	15.35	15.11	15.07	14.70	14.47

The values of $\bar{B}$ and $\int \frac{BdZ}{L}$ are in K-gauss and $\int \frac{HdZ}{L}$ in K-oersted

However, a study of an equivalent part of the magnet yielded the satisfactory result shown in Fig. 11. The vectors represent the magnitude and direction of the leakage flux at a height of 3 cm above the magnet, the leakage flux being the horizontal component of H_x and H_y.

It was clear from the figure that the obliquity of the lines of force within the useful region was not large, and thus the effect upon particle trajectories would not be serious.

CHAPTER 5

Characteristics of the Spectrograph.

5.1 The Geometrical Arrangement

The apparatus was designed to give comparatively high resolution in momentum and direction for the μ-mesons, together with a high particle rate. With this aim in view it was decided to use Geiger counters as detecting elements, with the possibility of later inclusion of neon flash-tubes (Gardener et al 1957, Ashton et al, 1960) to give even higher momentum resolution.

For the measurement of the variations of vertical flux the Spectrograph was set up as shown in Fig. 13. Particles were selected by three-fold telescopes, each comprising one counter in each of trays A, B and C. With this arrangement the counters in the trays A and B determined the direction of the particles, and those in tray C determined their displacement after passing through the magnet.

Referring again to Fig. 13, if the telescope consisted of counters in trays A, B and C set vertically above each other there would be 10 telescopes in all, each recording vertical, or nearly vertical particles of high momenta. Such particles were said to belong to

DIMENSIONS OF SPECTROGRAPH

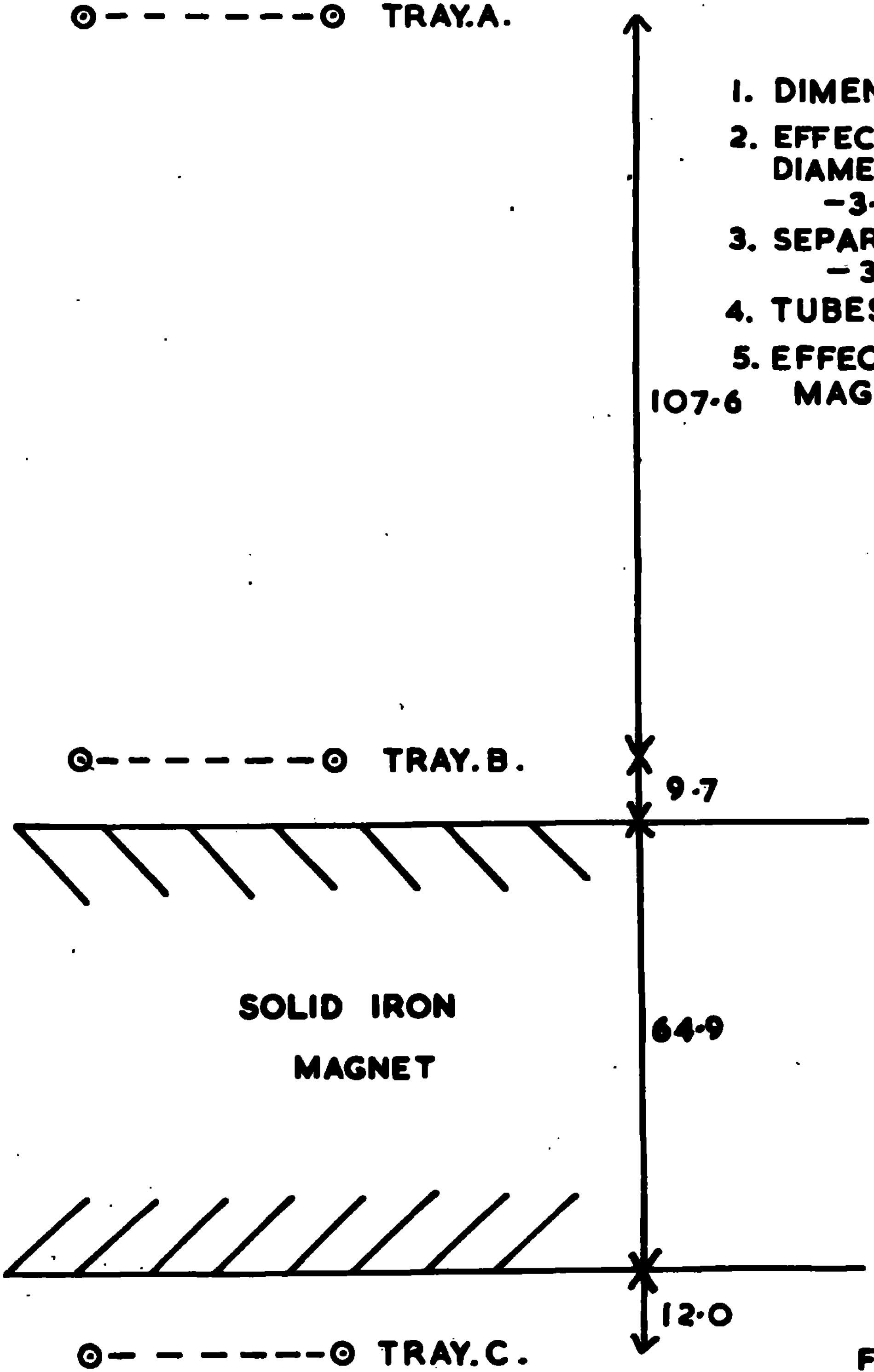

1. DIMENSIONS IN CMS.
2. EFFECTIVE (INTERNAL) DIAMETER OF TUBES: –3·32 cms.
3. SEPARATION OF TUBES: – 3·915 cms.
4. TUBES IN EACH TRAY: 10
5. EFFECTIVE WIDTH OF MAGNET: – 40 cms.

FIG.13

Category 111. If the counters in C were then displaced by one counter separation the category was said to be 110, or 112 depending on the direction of the displacement. Similarly Categories 113 or 220 referred to nearly vertical particles displaced by two counter separations in tray C.

The Geiger Counters used during the period of recording were manufactured by 20th Century Electronics Co. Ltd., Type G60. They were in fact conventional Geiger Counters, of sensitive length 60 cms, external diameter of the tube, 3.62 cm, and internal or useful diameter, 3.32 cm. In the Spectrograph the separation between adjacent counters was 3.915 cm.

5.2 The Acceptance Function of the Spectrograph

The particles selected by a telescope of particular configuration of counters as described in the previous section, do not possess a unique momentum but cover a band or spectrum of momenta, due to two main causes.

1. The finite size of the Geiger Counters.
2. The scattering of particles in their passage through the iron.

The basic problem that must now be solved is the determination of the momentum spectrum of the particles in each category. Let S(p) be the spectrum for a particular category, (p is the momentum), then the spectrum is given by the relation.

$$S(p) = N(p)A(p)$$

where N(p) is the differential μ-meson momentum spectrum incident at the top of the spectrograph N(p) has been determined to high accuracy over the important range by Owen & Wilson (1955) and more recently by Ashton et al (1960).

A(p) is termed the acceptance function of the spectrograph for particles of momentum (p), that is the relative probability of a particle of momentum p being accepted by the spectrograph. Referring to Fig. 13, it may be seen that the angles of inclination and deflection of the categories are small, thus making the derivation of an accurate solution quite simple.

For the derivation of this solution it is convenient at this stage to make two assumptions, as follows:

1. Negligible momentum loss by ionisation of the particle on passing through the iron.
2. Negligible scattering of the particles on passing through the iron.

The magnitude of the scattering is not in fact negligible but its effect, together with that of the loss of momentum of a particle on passing through the magnet can best be introduced at a later stage of the calculations.

It is apparent that any Category can be reduced to the Category 111 by displacing C an integral number of counter separations. The problem therefore resolves itself to the determination of the acceptance function for Category 111 only.

Consider Fig. 14(a); the internal diameter of each counter is b and the separation of the counter trays are as shown. A particle of momentum p undergoes a magnetic deflection ψ in passing through the magnet. A consequence of assumption (1), is that we can consider the particle to be deflected through the angle ψ at the centre of the magnetic field region; the deflection at O is therefore:-

$$\Delta = l_3 \psi$$

The probability of acceptance of particles of momentum p, that is of deflection Δ, $A(\Delta)$ is proportional to $\iint d\theta \, dG$ for all trajectories passing through A,B and C. The method of computing this integral can be

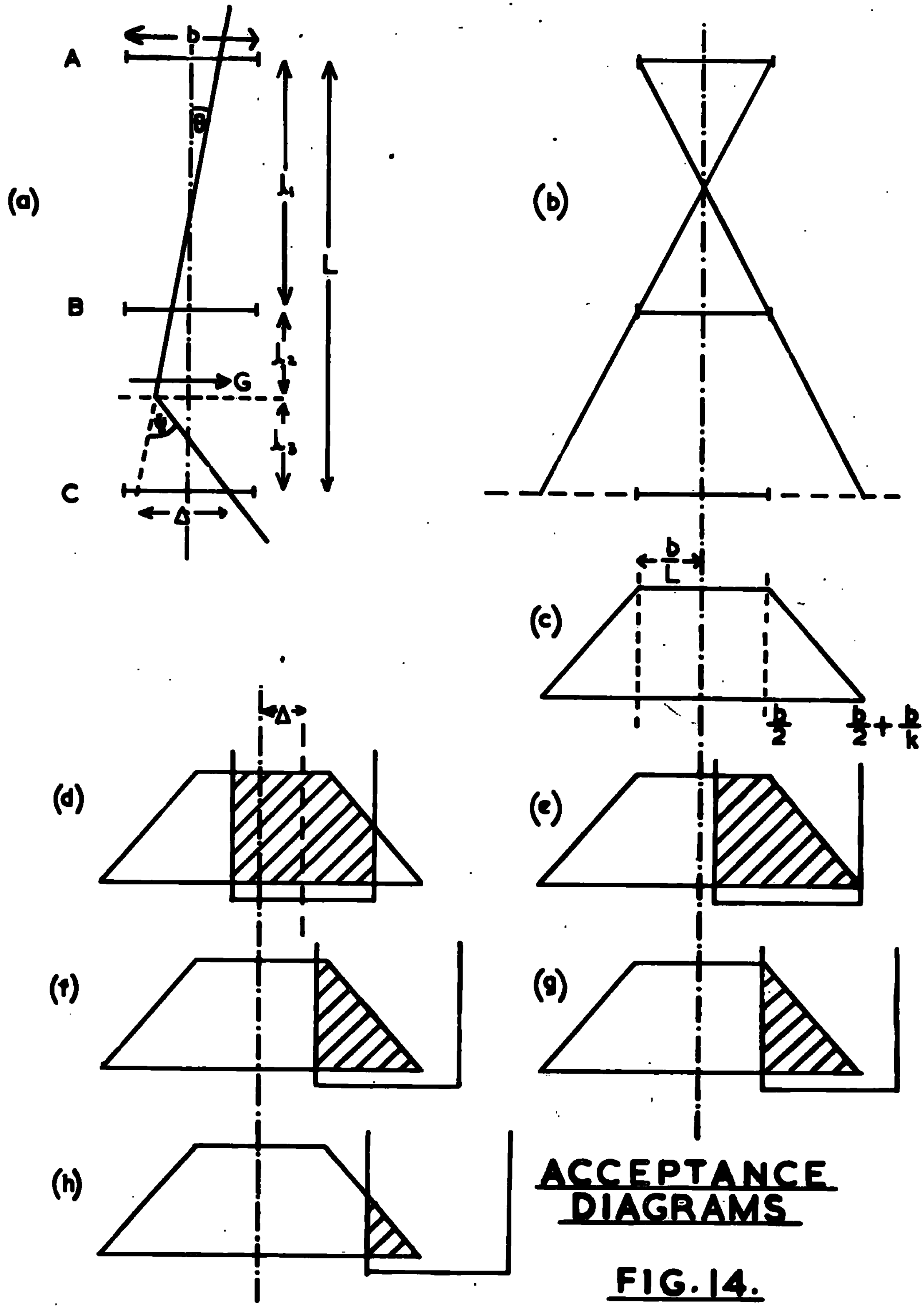

ACCEPTANCE DIAGRAMS

FIG. 14.

appreciated by considering the case of zero deflection.

1. $\Delta = 0$

The extreme trajectories are shown in Fig. 14 (b) for the case where the condition that the particles should pass through the counter C is disregarded. For an isotropic distribution of incident particles the distribution of particles at C is shown in Fig. 14 (c). This result can be seen by taking a point at C and determining the angle of acceptance set by the counters A and B. The co-ordinate of the curve is then the angle of acceptance and $\iint d\theta dG$ is the area under the curve. Simple geometry shows that the angle of acceptance falls to zero at a distance $\frac{b}{L} + \frac{b}{K}$ from the axis of symmetry, where

$$K = \frac{l_1}{l_2 + l_3} .$$

If now the condition that the counter in C be crossed is reimposed, the acceptance function is the area under the curve between $+\frac{b}{2}$ and $-\frac{b}{2}$

i.e. $\iint d\theta dG = \frac{b}{L} . b$ or rewriting $A_0(\Delta = 0) = \frac{b^2}{L}$.

2. $\Delta > 0$

Imposing a deflection on the trajectory is simply equivalent to displacing the centre in C by a deflection

The acceptance function is then the area of the curve cut off by the counter, as in the case $\Delta = o$.

As Δ increases several regions are covered, as represented by the diagram (d), (e), (f), (g) and (h) of Fig. 14. Thus (d) and (g) represent boundaries of regions and the remainder represent typical positions within the regions.

The acceptance functions have been computed for each region by finding the appropriate shaded area and the results for A(Δ) i.e. A, etc., are as follows:

$o \ll \Delta \ll \frac{b}{K}$; $A_1 = \frac{1}{l}\left(b^2 - \frac{K\Delta^2}{2}\right)$ diagram (d)

$\frac{b}{K} \ll \Delta \ll b$; $A_2 = \frac{1}{l}\left(b^2 - \frac{b^2}{2K} - b\Delta\right)$ diagram (f)

$b \ll \Delta \ll b + \frac{b}{K}$; $A_3 = \frac{1}{2Kl}\left(b + bK - K\Delta\right)$ diagram (h)

A method of checking these results is possible; the values of A agree for adjacent regions in the limiting case when Δ is equal to the boundary value. Agreement is in fact obtained.

The form of the variation of A(Δ) ($\propto A\left(\frac{1}{p}\right)$) is shown in Fig. 15 for Categories 11, 112 and 113. The abscissa is also given in terms of momentum,,p, for the case of the spectrograph operated at an excitation current of 16 amps.

ACCEPTANCE CURVES.

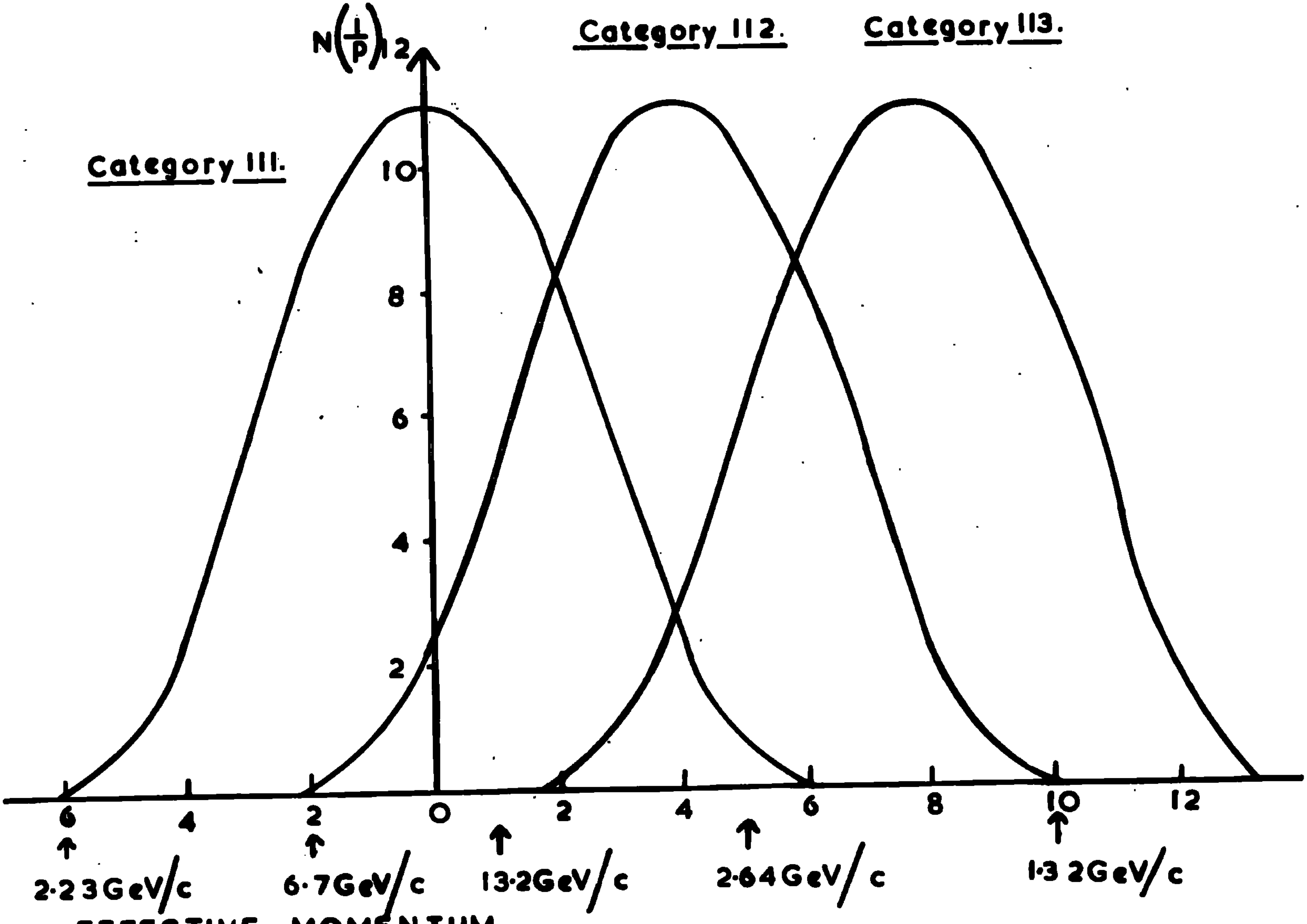

5.3 The Effect of Momentum Loss on the Acceptance Function

The unique relationship between p, the momentum of a particle, and its deflection in a magnetic field, together with the acceptance function for the spectrograph having been established, it becomes necessary to consider the two approximations upon which it is based, and to make such modifications as are necessary. The first of these assumes that the particle does not suffer any significant loss in momentum by ionisation in traversing the iron. In fact, it can be calculated that a particle on passing through 64.9 cm of iron will lose approximately 1 GeV. The effect of this loss of momentum is to cause a variation of the radius of curvature of the trajectory of the particle as on passing through the iron it will obey the relation

$$pc = 300\ B\rho \qquad \ldots\ldots\ldots\ldots \ (1)$$

where B is the total flux within the iron, which may be considered constant, and ρ is the radius of curvature of the trajectory. Considering the general case of vertical particles this variation in curvature will in turn affect the position and angle to the normal of the trajectory on its emergence from the iron. The situation is shown in Fig. 16. Trajectory (1) represents the path when momentum loss is neglected and (2) represents the

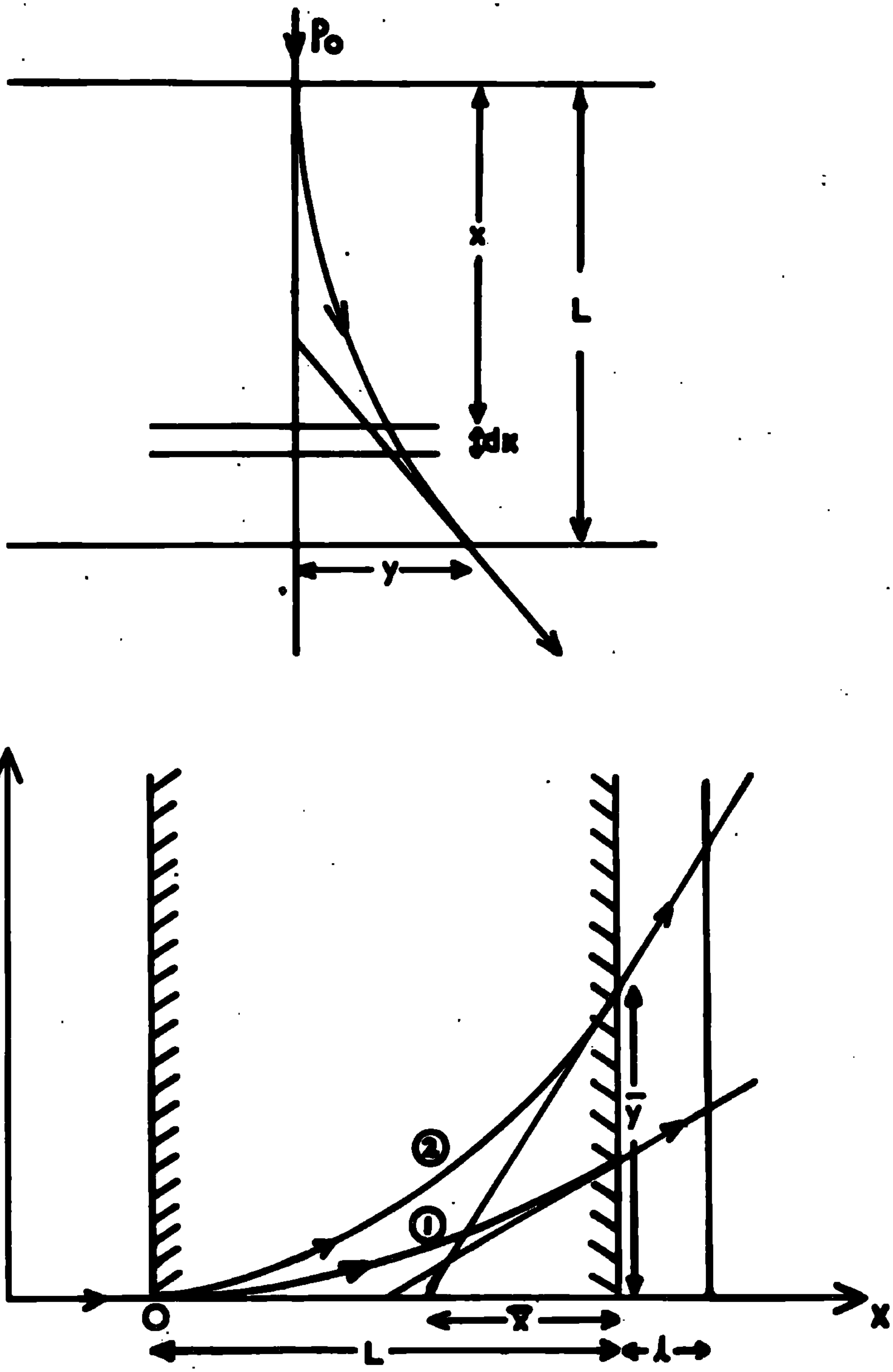

FIG. 16. VARIATION OF PATH THROUGH MAGNET DUE TO ENERGY LOSS

actual trajectory modified as it is by momentum loss (for reasons of clarity the effect has been greatly exaggerated).

The momentum of a particle at the instant that it has penetrated x cms through the magnet can be written to quite a high degree of accuracy as

$$p = p_o - \alpha x \qquad \text{.......(2)}$$

where p_o is the initial momentum of the particle and α the coefficient of loss per cm. Combining equations (1) and (2)

$$(p_o - \alpha x)c = 300\ B\rho$$

$$\text{i.e.} \qquad \rho = a - bx$$

where $a = p_o c/300$ B and $b = \alpha/300$ B.

Now it is well known that the radius of curvature of a trajectory at any one point may be represented by the relation

$$\rho = \left(1 + \left(\frac{dy}{dx}\right)^2\right)^{\frac{3}{2}} \bigg/ \frac{d^2y}{dx^2}.$$

Substituting in the above equation we obtain the general relation

$$\left(1 + \left(\frac{dy}{dx}\right)^2\right)^{\frac{3}{2}} = (a - bx)\,\frac{d^2y}{dx^2}. \qquad \text{.........(3)}$$

An attempt to solve this equation analytically proved unsuccessful, as it was found to require the integration of a cyclic function, which could only be achieved by laborious substitution. However it is possible to use the approximation

$$\left(1 + \left(\frac{dy}{dx}\right)^2\right)^{\frac{3}{2}} \longrightarrow 1$$

without introducing too much error

The result is the differential equation

$$\frac{d^2y}{dx^2} = \frac{1}{a - bx}$$

integration of which produced the relations

$$\frac{dy}{dx} = -\frac{1}{b}\log_e\left(1 - \frac{bx}{a}\right) \qquad \text{........(4)}$$

$$y = \frac{1}{b^2}(a - bx)\log_e\left(1 - \frac{bx}{a}\right) + \frac{x}{b} \qquad \text{........(5)}$$

Substituting for a and b and expanding the logarithmic terms gives the diminishing series:

$$\frac{dy}{dx} = \frac{300Bx}{p_0c}\left\{1 + \frac{1}{2}\left(\frac{\alpha x}{p_0c}\right) + \frac{1}{3}\left(\frac{\alpha x}{p_0c}\right)^2 + \frac{1}{4}\left(\frac{\alpha x}{p_0c}\right)^3 + \cdots\cdots\right.$$

$$y = \frac{300B}{2p_0c}\cdot x^2\left\{1 + \frac{1}{3}\left(\frac{\alpha x}{p_0c}\right) + \frac{1}{6}\left(\frac{\alpha x}{p_0c}\right)^2 + \frac{1}{10}\left(\frac{\alpha x}{p_0c}\right)^3 + \cdots\cdots\right.$$

A check on the validity of this relation may be obtained by returning to the case of no energy loss. This may be done by considering the point at which all the deflection of the particle may be considered to take place. From Fig. 16 it may be seen that this point, designated $\bar{x}$ is obtained from

$$\bar{y} \Big/ \frac{d\bar{y}}{dx} = \frac{300\,BL^2}{2p_oc} \cdot \frac{p_oc}{300\,BL} = \frac{L}{2}.$$

which is geometrically true.

The validity of the functions having been established it is possible to compile the following Table comparing the results obtained for the two cases for a variety of values of initial momentum ranging from 1.25 GeV/c to 50 GeV/c, this covering the whole range of the various energy spectra considered.

It can at once be ascertained from the Table that for values of incident momentum between 50 GeV/c and 5 GeV/c, neglecting the momentum loss does not appreciably affect the trajectory of the particle, and hence the probability of being accepted by a certain category, but that for particles of momentum below the lower limit the error becomes very large.

TABLE V

The Effect of Momentum Loss on Particle Displacements.

	Consideration without loss		Consideration with loss			
p_oC Gev/c	disp.l at x = L	(cms)	disp.l at x = L	(cm)	Difference (cm)	% difference
1.25	7.84	10.72	11.67	17.45	6.73	38.0
1.5	6.55	8.96	8.75	12.68	3.72	29.0
1.8	5.44	7.45	6.80	9.75	2.30	24.0
3.0	3.26	4.46	3.70	5.16	0.70	13.5
5.0	1.96	2.68	2.10	2.91	0.23	7.9
10.0	0.98	1.34	1.01	1.39	0.05	3.6
20.0	0.49	0.67	0.50	0.68	0.01	1.5
30.0						
40.0						
50.0	0.20	0.27	0.20	0.27	-	-

A simpler approach can be tried in order to get sufficiently accurate results for the trajectory including momentum loss. Instead of using the initial momentum of the particle the mean (effective) momentum of the particle, as it passes through the magnet, may be tried. This is given by

$$p_{eff} = \tfrac{1}{2}\ p_o + (p_o - \alpha L)$$

$$\text{i.e.}\quad p_{eff} = p_o - \tfrac{1}{2}\alpha L$$

$$= p_o - 0.5. \quad \text{with the p's in GeV/c.}$$

Table VI below again covers the whole range of the momentum spectrum, and shows the effect of the modification and it may be seen that to an accuracy of better than 6% this modification may be justified over the whole of the momentum range considered.

TABLE VI

The Accuracy of the Approximate treatment of Momentum Loss

p_oc	$p_{eff}c$ GeV/c	approx	with loss	difference (cm)	difference in %
1.25	0.75	17.9	17.45	0.45	2.6
1.5	1.0	13.4	12.68	0.72	5.7
1.8	1.3	10.3	9.75	0.55	5.6
3.0	2.5	5.46	5.16	0.30	5.8
5.0	4.5	2.98	2.91	0.07	2.4
10.0	9.5	1.41	1.39	0.02	1.4
20.0	19.5	0.68	0.68	-	-
30.0	29.5	0.41	0.41	-	-
40.0	39.5	0.33	0.33	-	-
50.0	49.5	0.27	0.27	-	-

5.4 Effect of Scattering on the Acceptance Function

The second approximation made in calculating the acceptance function was the neglect of the effect of Coulomb scattering of the μ-mesons in the iron. As with the previous case of momentum loss this approximation is not strictly true and it is now necessary to make some allowance for scattering.

Consider a particle of momentum p_o and velocity βc incident normally on the magnet and traversing it as shown in Fig. 17 (a). It is required to find the r.m.s. displacement $\langle Z \rangle$ due to scattering alone at a level distance x_2 below the magnet, where in the present case $x_2 = 1$. Consider the contribution ΔZ which arises from an elementary deflection $\Delta\theta$ occurring in a thickness dx, distance x below the top of the magnet, as shown in the figure.

ΔZ is given by the relation

$$\begin{aligned}\Delta Z^2 &= (x_2 - x)^2 (\Delta\theta)^2 \\ &= (x_2 - x)^2 K^2 dx / p^2 \beta^2\end{aligned}$$

where K is the scattering constant.

SCATTERING IN SOLID IRON SPECTROGRAPH

FIG. 17a.

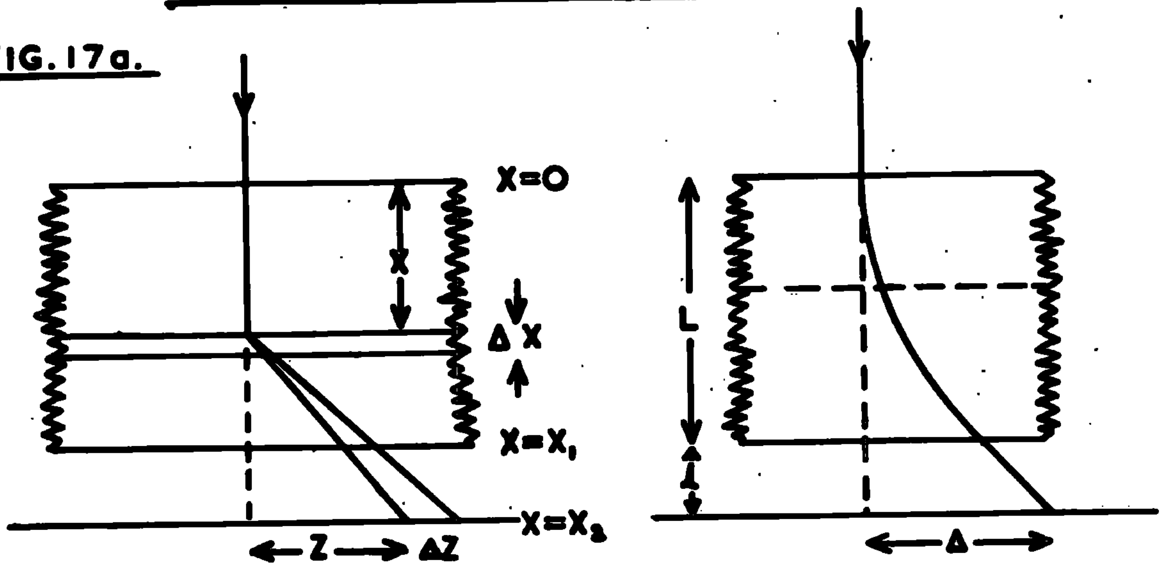

FIG. 17b.

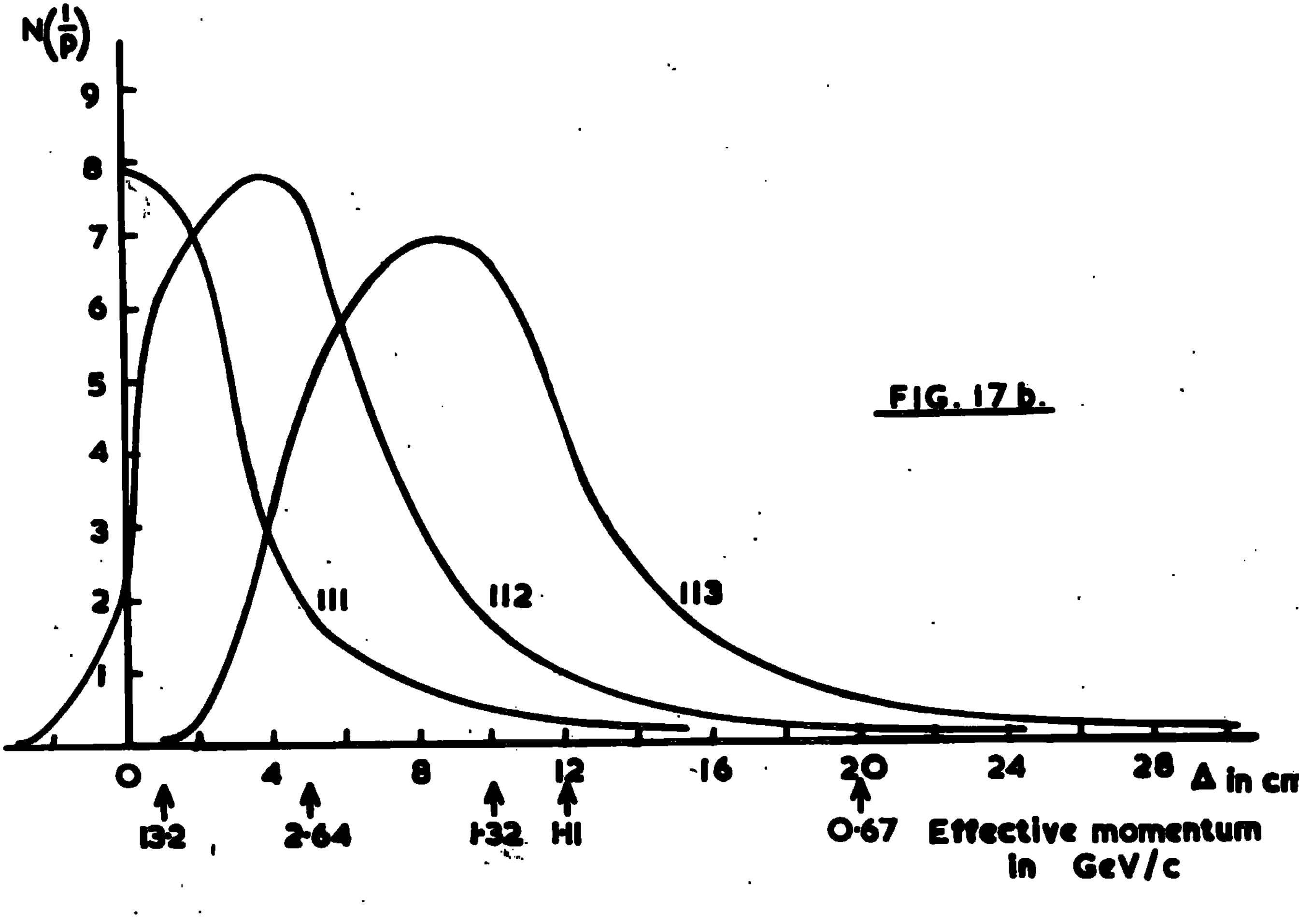

It is therefore possible to integrate over the whole of the region of the magnet from x = o to x = x, to find an expression for the mean square displacement $\langle Z\rangle^2$.

Thus

$$\langle Z\rangle^2 = \frac{K^2}{p_0^2\beta^2}\int_0^{x_1}(x_2-x)^2\,dx.$$

$$= \frac{K^2}{p_0^2\beta^2}\left[-\frac{(x_2-x)^3}{3}\right]_0^{x}$$

$$= \frac{K^2}{p_0^2\beta^2}\left\{3x_1x_2(x_2-x_1)+x_1^3\right\}$$

Substituting in the above expression for x_1 = L and x_2 = L + l we obtain

$$\langle Z\rangle = \frac{K}{p\beta}\cdot\frac{1}{\sqrt{3}}\left\{L\sqrt{L+3l\left(1+\frac{l}{L}\right)}\right\}$$

This equation shows that the r.m.s. deflection $\langle Z\rangle$ is inversely proportional to the incident momentum p_o of the particle at high velocities, where $\beta = 1$.

It is necessary to find a value for the factor K, the scattering constant, and to this end the present case was compared with the results found by Lloyd and Wolfendale (1955) on the scattering of μ-mesons in iron. This gave, introducing the appropriate factor for the thickness of the magnet, the value of K is found to be 1.152 x 10^{-2} GeV/c.$\text{cm}^{-\frac{1}{2}}$.

The effect of scattering is to superimpose on the magnetic deflection Δ_0 (= $\frac{\text{constant}}{p}$) a Gaussian error of standard deviation $\langle Z \rangle_p$ so that particles of momentum p have a range of deflections given by

$$N(\Delta)d\Delta = \frac{1}{\sqrt{2\pi}\langle Z \rangle_p} \exp \frac{-(\Delta-\Delta_0)^2}{2\langle Z \rangle_p^2} . d\Delta$$

The modified acceptance function is now found by using this distribution in Δ in the analysis described in section 5.2. This had been performed for categories 111, 112, 113, the important categories in the present work with the results shown in Fig. 17(b). The area under the curves corresponding to the total probability of accepting a particle will remain constant.

By comparison of Fig. 17b with Fig. 15, where scattering is neglected, it will be observed that the effect of scattering is to reduce somewhat the most probable momentum for each category and to add a low momentum 'tail' to each momentum distribution.

5.5 The Momentum Spectra for the Various Categories.

As stated in section 5.2 the momentum spectrum of particles in each category S(p) is given by

$$S(p) = N(p)A(p)$$

where N(p) is the differential μ-meson momentum spectrum incident at the top of the spectrograph. N(p) has been taken from the spectra measured by Owen and Wilson (1955) and by Ashton et al (1960), and the resultant spectra S(p) are given in Fig. 18. As would be expected the spectra sharpen considerably as the mean deflection is increased. A useful characteristic is the median momentum for each category, and values found from the figure are given in Table VII. (The values for the median momentum neglecting the effects of scattering are also included for comparison).

TABLE VII

The Median Momentum for each Category

Category	Median momentum in GeV/c	
	Neglecting scattering	Including Scattering
111	8.6	9·1
112, 110	4.5	5·0
113, 220	2.9	3·4

When considering the momentum spectra, as presented in Fig. 18, and the modifications to the acceptance function as presented in the two previous sections, it must be remembered that the treatment is not rigorous as

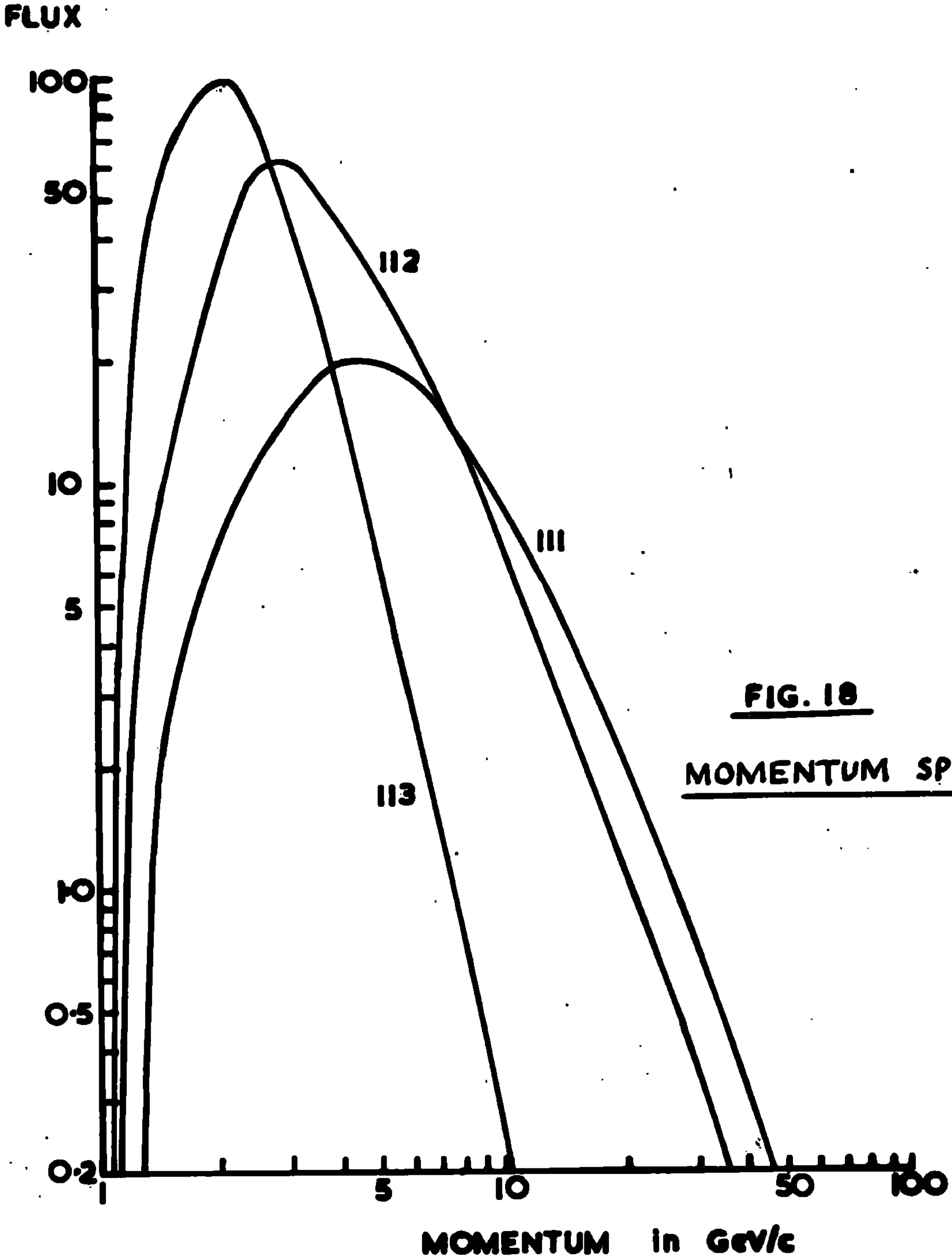

FIG. 18

MOMENTUM SPECTRA

the two effects of energy loss and scattering act at the same time and not independently, as has been assumed. The treatment presented, however, is considered to be accurate to within a few per cent and therefore sufficiently precise for the study of the meteorological coefficients, which vary only slowly with momentum.

CHAPTER 6

The Electronic Circuits.

6.1 The 'Vertical Spectrograph'

As mentioned already the particles are selected by 3-fold telescopes, each comprising one counter in each of layers A, B and C (Fig. 13). A block diagram of the electronic circuits required to obtain this selection is shown in Fig. 19. It will be seen that the outputs of the coincidence circuits are added together and the total number of particles is recorded every 25 minutes. The timing circuit devised to facilitate this automatic recording is shown in Fig. 22.

The electronic circuits are of simple design, the emphasis being on complete reliability; the circuit diagrams are shown in Figs. 20, 21 and 22. Some saving in cost and improvement in reliability was affected by the use of double-triode valves in several parts of the circuits. This was done as shown in the case of the Quenching Units (Fig. 21), which were required, in the case of trays B and C, to work in close proximity of the magnet, with its associated problems of heat conduction. In spite of working in temperatures considerably in excess of the ambient temperature (15°C) the circuit proved of high reliability, only 2% of the total record-

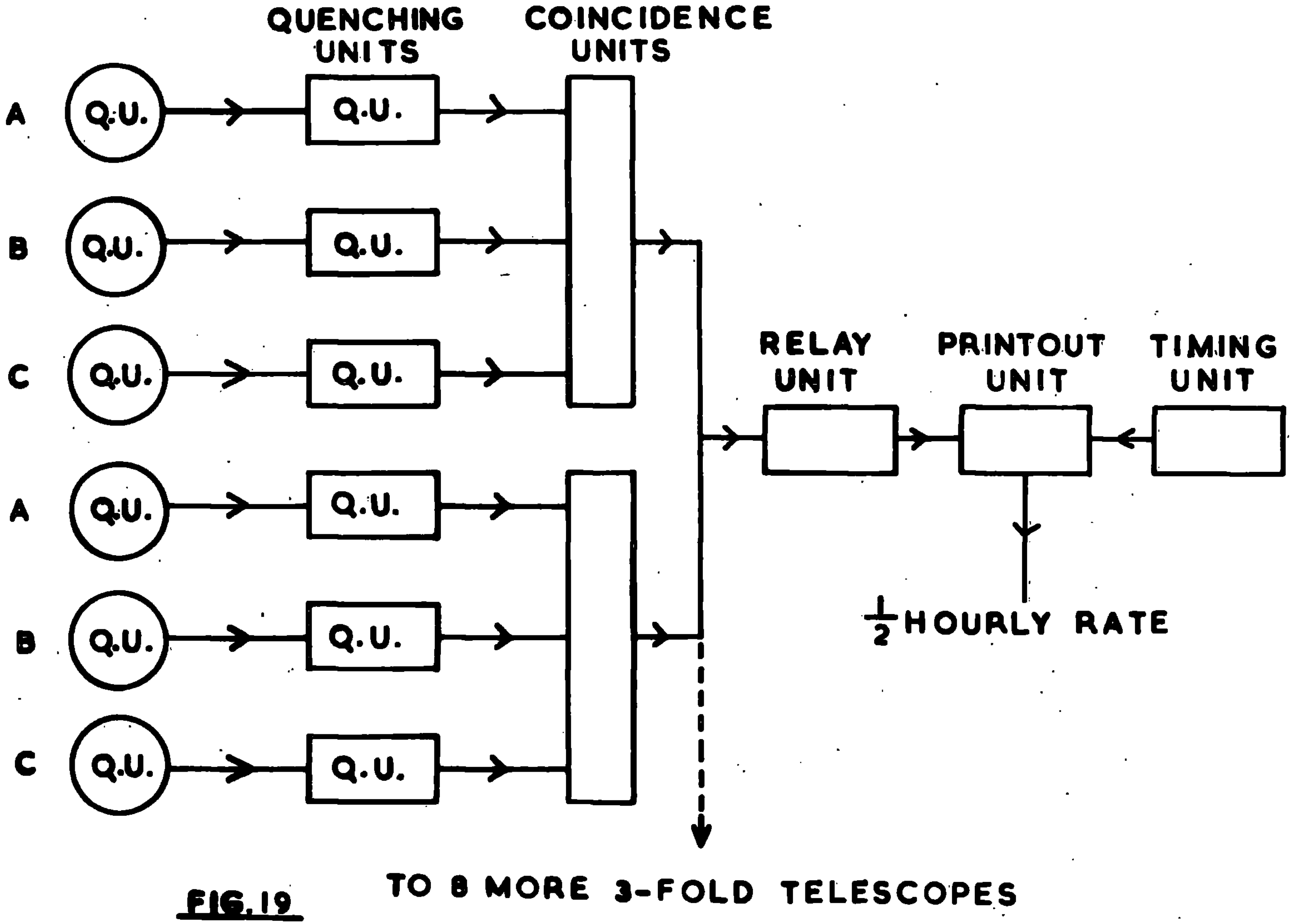
BLOCK DIAGRAM OF CIRCUITS

FIG. 19

COINCIDENCE CIRCUIT.

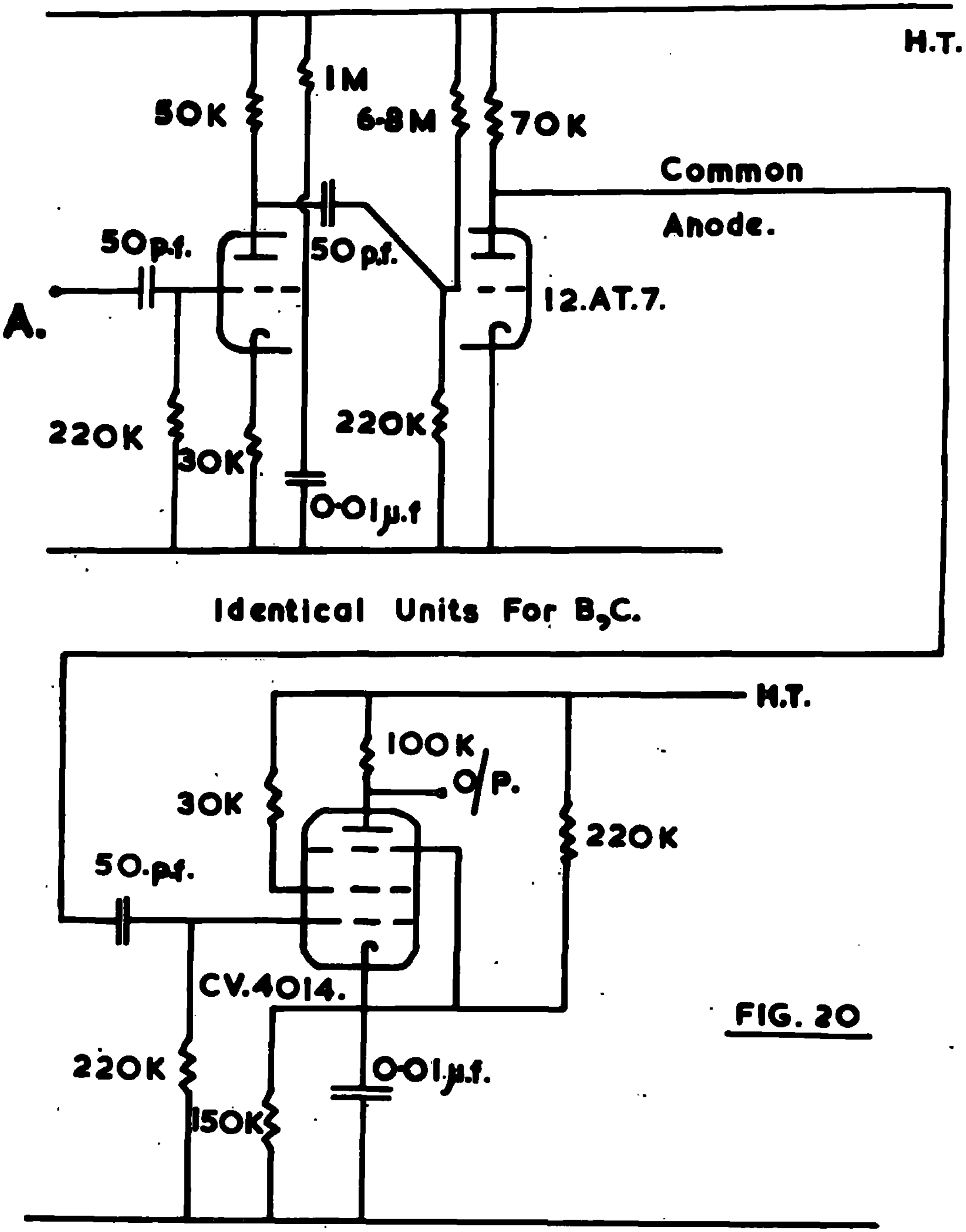

FIG. 20

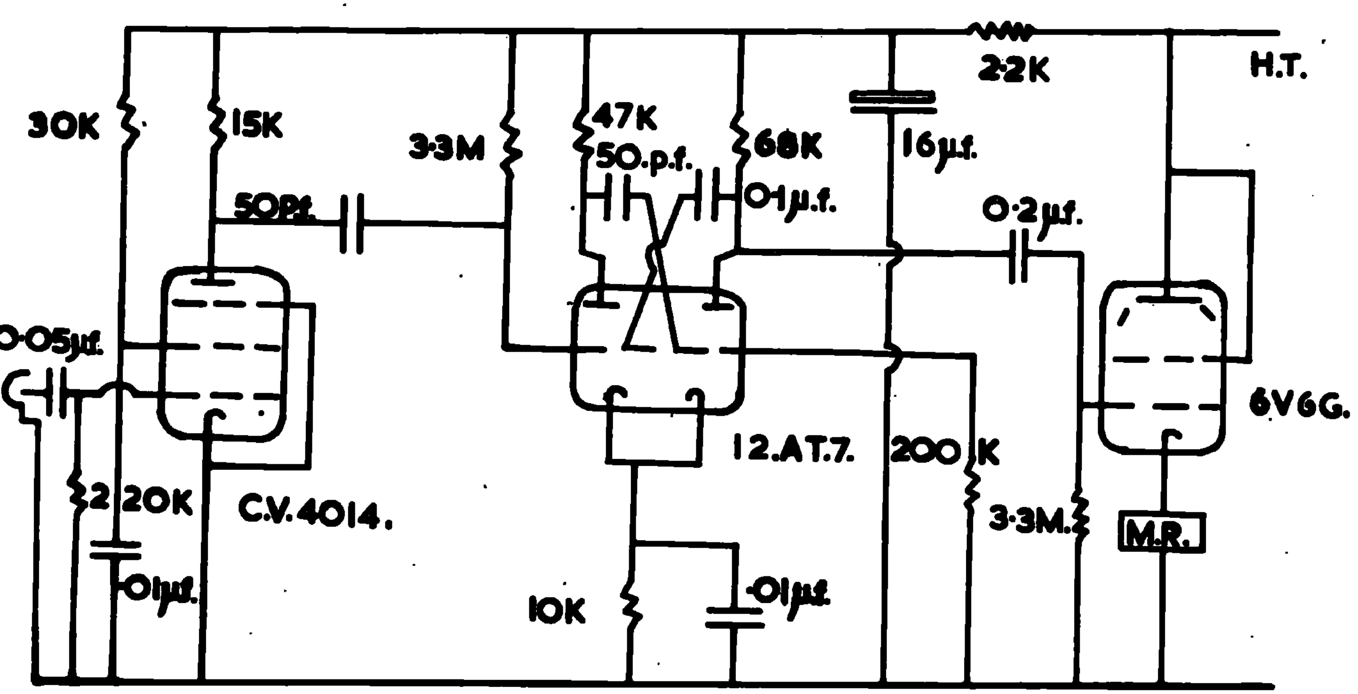

MESSAGE REGISTER CIRCUIT.

QUENCHING UNIT CIRCUIT.

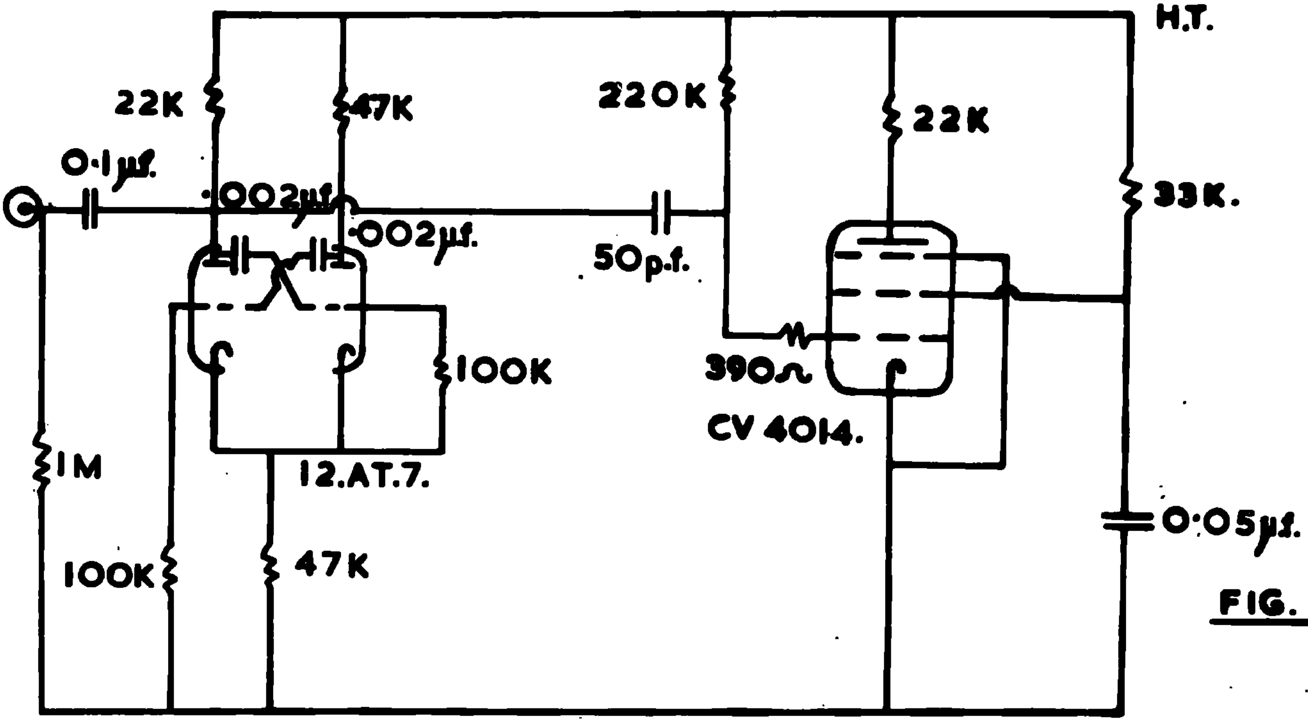

FIG. 21

TIMING CIRCUIT

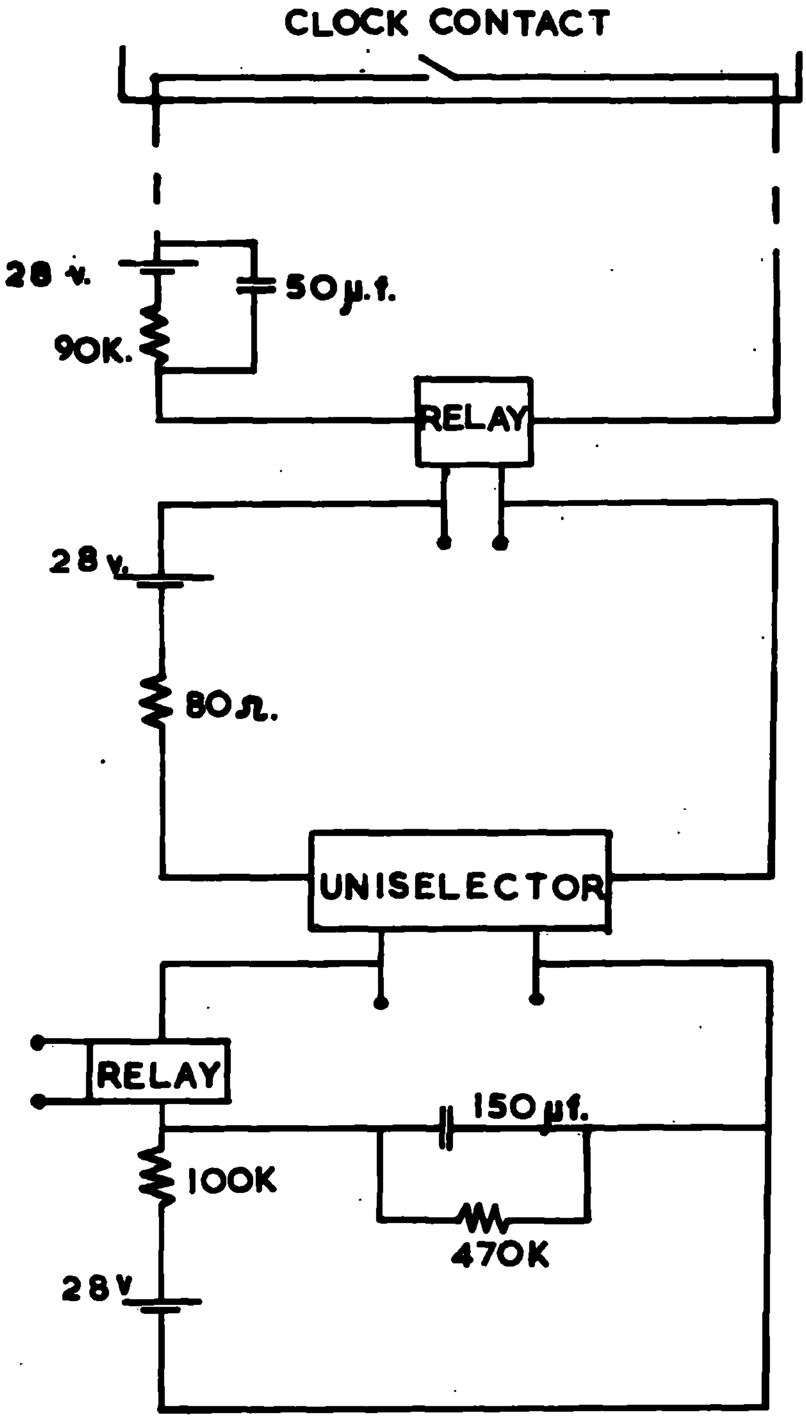

FIG. 22

ing time being lost due to Quenching Unit failure, although care had to be exercised in the choice of the individual double-triodes, the characteristics of some rendering them liable to free-running.

The coincidence circuit also incorporates double-triodes for reliability, proving only slightly less effective, 6% of total recording time being lost due to coincidence circuit failure; in this case however the circuit does not demand such exacting working characteristics from the double-triode. The majority of the rest of the recording time lost (~10%) was due to the deterioration of the electrolytic condensers in the timing circuit. The electronic circuits therefore proved in all 85% efficient, the majority of the failures occurring in the early days of operation.

6.2 Modifications for Horizontal Recording

The modification of the apparatus for the eventual study of particles in the near horizontal direction can also be usefully discussed here. The flux of μ-mesons at sea-level in a horizontal direction is low in comparison with the vertical flux, thus without exclusion simultaneous particles in the vertical plane (i.e. from extensive air showers) the true horizontal rate would be masked. This exclusion was affected electronically by the introduction of a second coincidence circuit with the former shown in Fig. 19. This latter circuit (Fig. 23) recorded the simultaneous discharge of any two or more counters in any tray together with discharges in the other two trays, and therefore recorded the number of shower events. Subtraction of this rate from the total rate of 3-fold coincidences gives the rate of single unaccompanied particles, thus excluding the possibility of a vertical particle.

A second modification introduced to increase the total rate for categories other than 111, was to increase the number of Geiger Counters in trays A and C, to 12 in the former, and 14 in the latter case. This was done because it is not practicable once the trays have been positioned to move them in a vertical plane.

With these modifications it should prove possible to study the variations of intensity of cosmic rays near the horizontal direction.

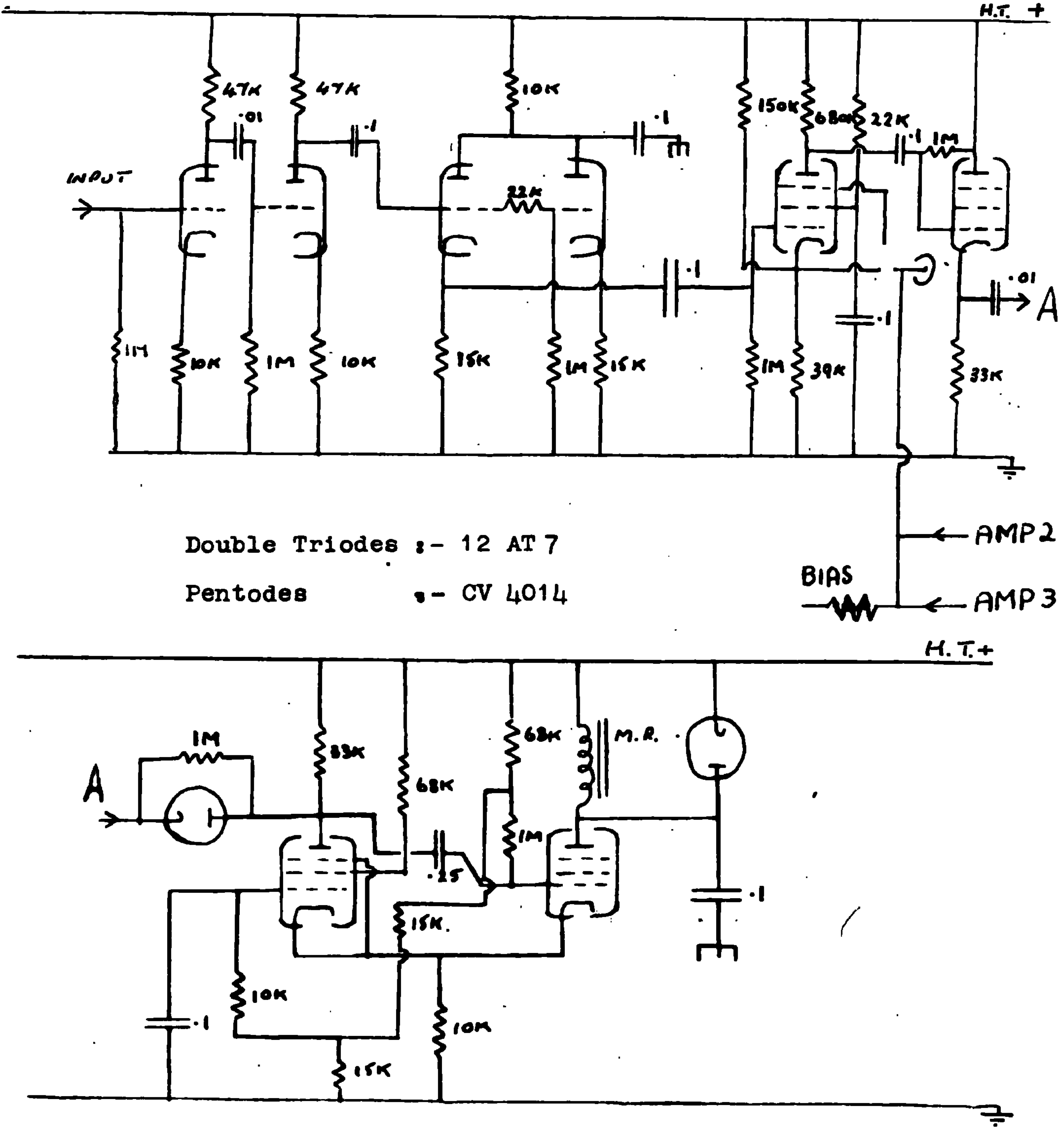

Double Triodes :- 12 AT 7

Pentodes :- CV 4014

FIG. 23. Horizontal Recording, coincidence circuit for recording of shower components.

CHAPTER 7

The Experimental Results on Intensity Variations in the Vertical Direction

7.1 The basic data on particle rates

As has been mentioned already the number of particles traversing the spectrograph was recorded automatically every 25 minutes. These numbers were printed out on paper, on which was also noted, at convenient intervals, the date and time. The spectrograph was operated for an extended period on each of the categories given in Table VIII, 40 separate records, involving 70,000 particles being recorded for category 111, and 10 separate records for each of the other categories mentioned; recording over 10,500 particles in each case. The particle rates and median momentum for each Category are also given in Table VIII.

TABLE VIII

CATEGORY	Median Mom. in GeV/c.	Rate of Particles in counts/hr.
111	9.1	72.7
110, 112	5.0	60.6
220, 113	3.4	43.3

Throughout the whole of the period of recording the excitation current of the magnet was strictly monitored using a recording milliammeter, to ensure that the current variation remained within the appropriate limits (see section 4.3), that is to a standard deviation of 1.5%.

Alternate records were obtained with the sign of the current through the excitation coils reversed, thus causing the spectrograph to accept particles still within the same energy spectrum as defined in Fig. 18, but of the opposite sign. Within any one category it was therefore possible to quickly check the validity of each day's recording by comparison with its predecessors; firstly with the total number of particles recorded so far, and secondly the ratio of the number recorded to those of the opposite sign recorded on the previous day. With these checks it was possible to locate any large-scale discrepancies caused by, for example, failures of Geiger counters or the electronic circuits. When failures were detected the record for that day was deleted.

A number of tests were carried out to check that the apparatus was counting the desired events, viz. 3-fold coincidences. For example, a frequent check of the discriminations of the coincidence circuit was performed by 'feeding in' a very high rate of 2-fold coincidences and ensuring that none of these events was able to break-through the circuit and be recorded as 3-fold events.

A further check concerned the question of the time relationship of the accepted 3-fold events. It is normally assumed that the particles obey the Poisson statistics; for example this is assumed when the standard deviation of n events is taken as $\sqrt{n}$.

This check was made by recording the time interval between successive particles. Fig. 24 represents the frequency distribution for 2,000 particles, for which the mean time interval was $\tau = 44.6$ seconds. The diagonal line represents the curve calculated for a Poisson distribution for this mean interval. It will be seen that the relation holds true over the whole of the range considered, even to the longest time intervals, for which few particles were recorded.

7.2 The Meteorological Data

The meteorological data used in the analyses was

FREQUENCY DISTRIBUTION OF INTERVALS BETWEEN PARTICLES

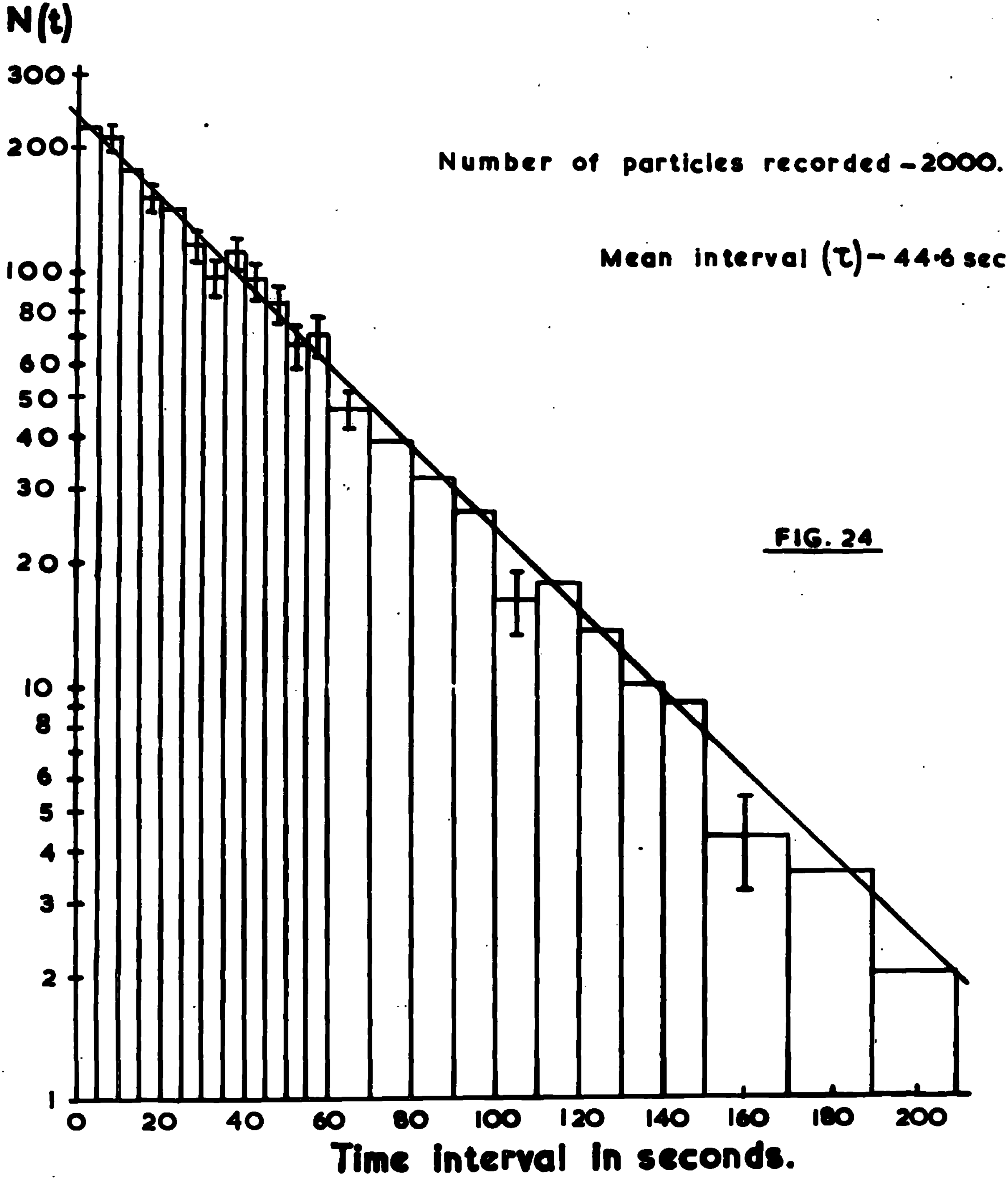

Number of particles recorded – 2000.

Mean interval (τ) – 44·6 sec

FIG. 24

obtained from the Meteorological Office, who publish data found from radiosonde observations from a number of stations in Britain. The nearest station to Durham is Leuchars, some 120 miles to the north.

Before the data obtained from Leuchars could be used however it was necessary to study the effect that this distance would have on the accuracy of the data, as applied to Durham. To enable this to be done, the data from 3 Meteorological Stations was studied and compared; Leuchars, Hemsby about 130 miles south-west of Durham, and Aughton about the same distance to the south-east, as shown in Fig. 25. Thus Durham lies roughly equidistant from these 3 stations, in the centre of the triangle formed by them, and any variation of parameters from station to station could be considered to include any variation at Durham.

A close study of the data from these 3 stations, carried out over a period of days, and including the variations of temperature and pressure levels up through the atmosphere revealed little significant change from station to station; thus it was concluded that for the present study the data obtained from Leuchars was satisfactory, and that a detailed study of the variation in intensity of the μ-meson with the atmospheric parameters could be carried out.

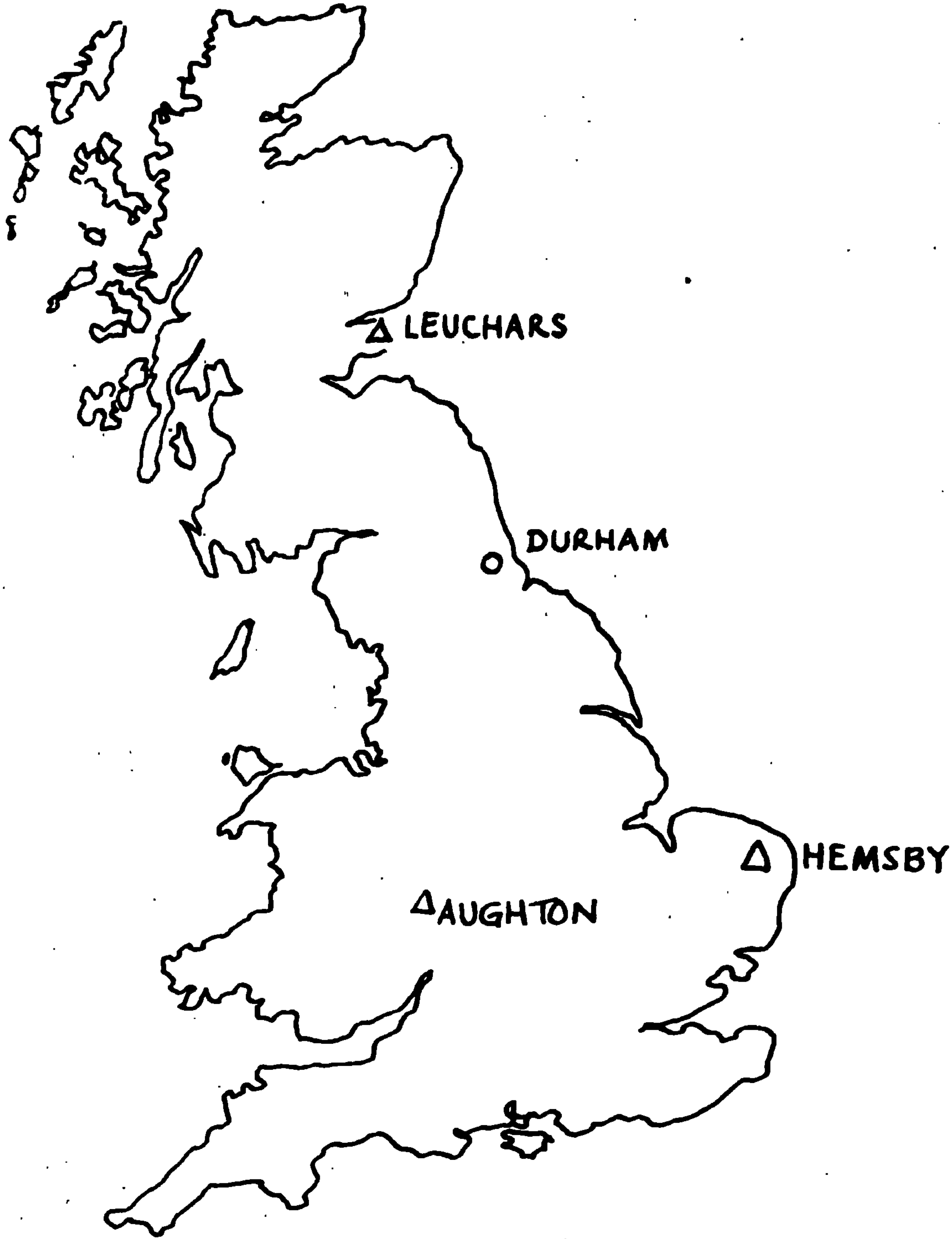

FIG. 25 Meteorological stations 'near' Durham.

The meteorological data abstracted for use in the analysis comprised the following:

(i) the sea level pressure

(ii) the heights of the 100 mb and 150 mb levels

(iii) the atmospheric temperatures at sea level and at the 500 mb, 200 mb, 150 mb and 100 mb levels.

The rate of particles was found for 4-hourly periods and was plotted against time, along with the meteorological parameters given above. Attempts at correlation were then made as described in the next Chapter.

7.3 The Day-Night Particle Rate for Each Category.

From the treated data described in the previous section it was possible to obtain the mean rate for each 4-hourly period of the day, for each of the three particle energy bands under consideration. Thus it was possible to divide all the particles into 2 groups; those that occurred during the day-time, when the sun was over the horizon, and those that occurred at night. Table 9 represents the results of this treatment, together with the results that have been obtained from Glaser et al (1950) (referred to in Section 2.5). It may be seen that although the two experiments give reasonable agreement for mean energies of 9.1 and 5.0 GeV/c, for the lower mean energy of 3.4 GeV/c there is a significant discrepancy between the two sets of results. It is important to note however that a vigorously direct comparison is not possible; the results of Glaser et al (1950) represent the measurement of a maximum of 200 particles of an exact energy, whereas Category $\frac{113}{220}$ represents the recording of 20,000 particles within an energy band defined by Fig. 18. The conclusion that can be drawn from this work is that there is no evidence in favour of the large diurnal variation found by Glaser et al, at least for momenta above about 2 GeV/c.

TABLE 9

The Day-Night Particle rate for each Category

CATEGORY	MEAN ENERGY (GeV/c)	MEAN DAY-NIGHT RATE (% of total particles recorded)	
		DURHAM	GLASER ET AL
111	9.1	-1.3 ± 0.15	0 ± 11
110 112	5.0	-1.2 ± 0.3	-4.0 ± 6.5
220 113	3.4	+1.45 ± 0.45	-10 ± 4.5

CHAPTER 8

Correlation of the Intensity Variations with Meteorological Parameters

8.1 General Considerations

It is convenient to discuss the analysis of the results in order of increasing complexity. Thus, there will firstly be considered the simple partial correlation of intensity with sea level pressure i.e. the determination of the 'pressure coefficient' and then will follow a more detailed treatment of the correlation with the various parameters.

8.2 Correlation with pressure

The correlation of intensity with sea level pressure has been studied in a straightforward way by splitting up the pressure range into convenient intervals and finding the average counting rate for each interval, Fig. 26 shows the results for two categories; the correlation between rate (intensity) and pressure is quite marked, although the statistical errors are large.

It is usual to write the correlation coefficient as a_p = percentage change in intensity per mb change in sea level pressure. Values of a_p for each of the categories are shown in Fig. 27, plotted as a function of the

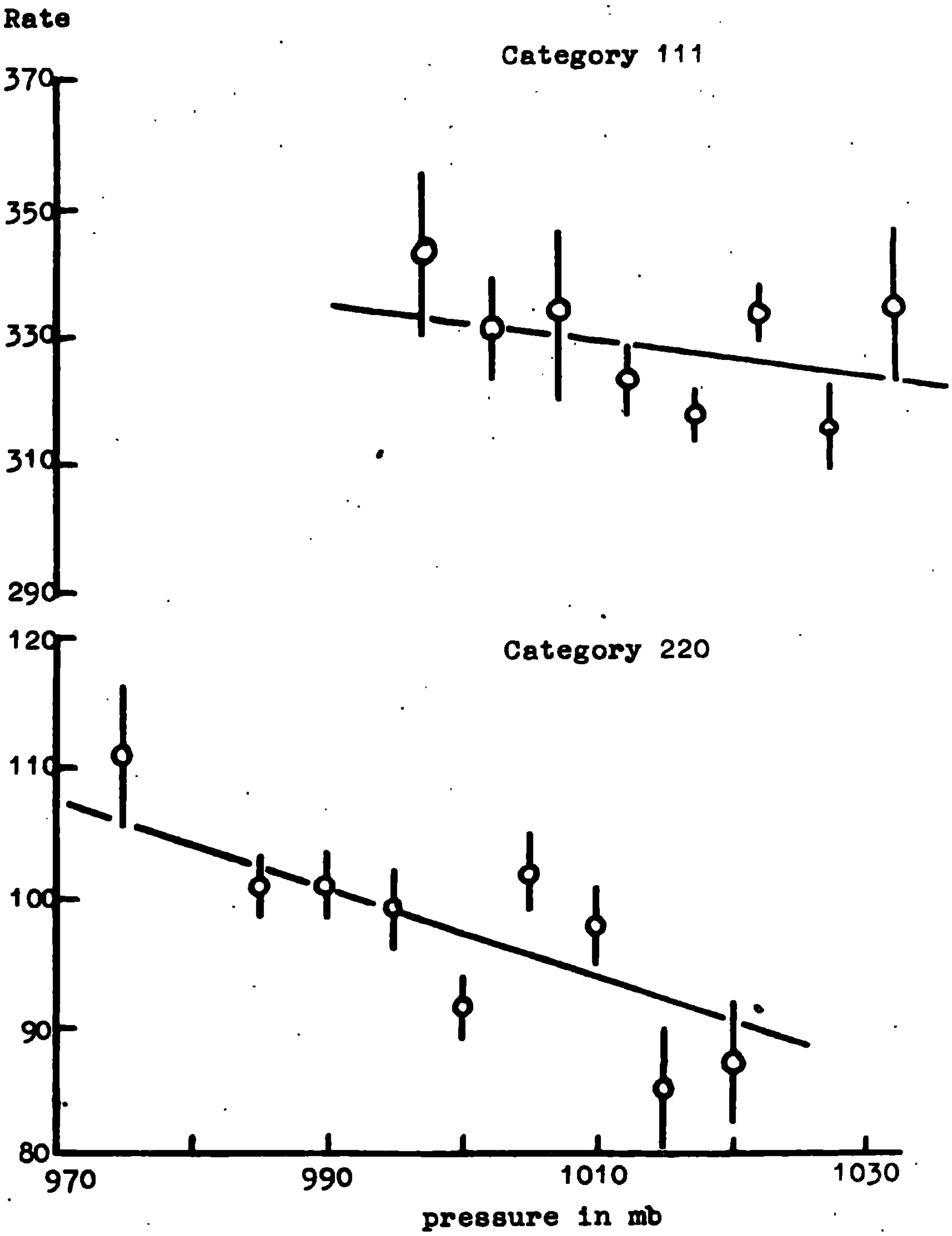

Fig.26. The Variation of Rate with Pressure

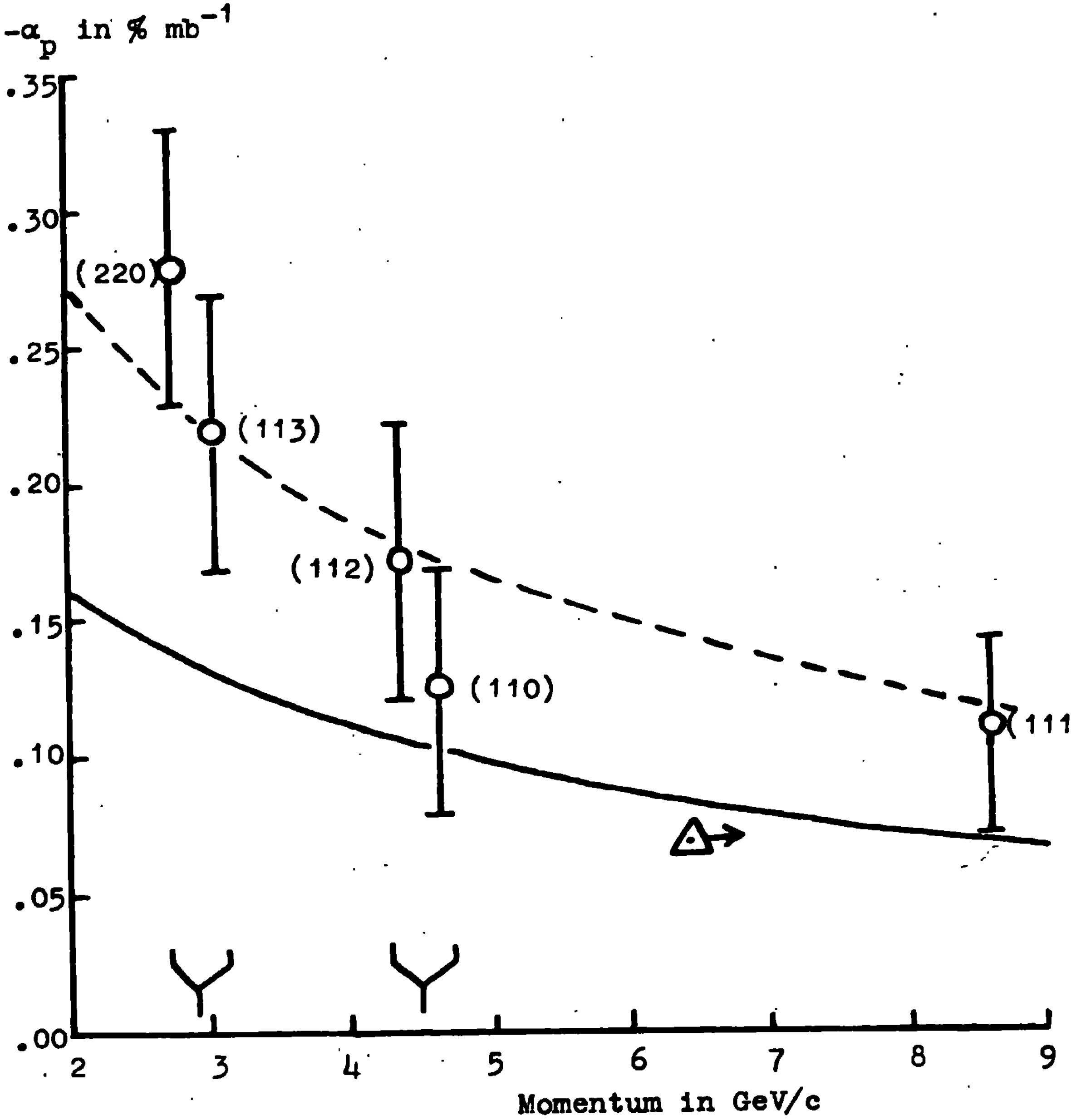

Variation of Pressure Coefficient with Momentum

Fig. 27

median momentum (Table 7).

Also shown in Fig. 27 is the theoretical relationship due to Olbert (1954). The point shown as a triangle refers to an integral momentum spectrum, as calculated by Dorman (1957). The consistency between these points and the theoretical curve of Olbert is reassuring.

It is seen that the points found from the present measurements are consistently higher than expectation. This is just what would be expected if, during the period of the experiment, there had been correlation between the pressure changes and changes in the other meteorological parameters. An increase in ordinate by a factor of 1.7 brings about good agreement between experiment and theory - the scaled up curve is also shown in Fig. 27.

8.3 Application of the Correlation Treatment of Dorman

As was mentioned in §2.3 a comprehensive treatment of the correlation problem has been given by Dorman (1957). This author has pointed out that the fundamental meteorological factor which is intimately connected with the barometric pressure is the atmospheric temperature. Thus, most of the troposphere is usually warmer under high pressure and colder at low pressure; in both cases there will be an enhanced variation in cosmic ray intensity and an apparent increase in the pressure coefficient.

Following Dorman, the effect of temperature variations (at constant pressure) can be considered as follows: The relative variation in the intensity of μ-mesons, $\frac{\delta N_\mu}{N_\mu}$, due to variations in air temperature $\delta T(h)$ in the region from the top of the atmosphere to the level of observation, h_o, may be represented in the form

$$\frac{\delta N_\mu}{N_\mu} = \int_0^{h_o} W_T(h)\,\delta T(h)\,dh.$$

where $W_T(h)$ is a function indicating the role of the various layers of air in the production of the temperature effect on a 1°C variation in the air temperature. $W_T(h)$ therefore represents the 'density' of the temperature coefficient.

Dorman shows that $W_T(h)$ varies strongly with the level of observation, h_o, the π-meson production spectrum and the minimum energy of recorded μ-mesons $\Delta\mathcal{E}$.

It is now necessary to find the value of this integral for the periods of time for which data for each pressure range (§8.2) was accumulated and to correct each intensity. The result will then be a corrected mean intensity for each pressure range, from which the corrected pressure coefficient may be found directly.

The variation of $W_T(h)$ with h was calculated by Dorman for $\Delta\mathcal{E}$ = 0.4, 6.4 and 14.4 GeV with the result shown in Fig. 28. For the present work the variation is

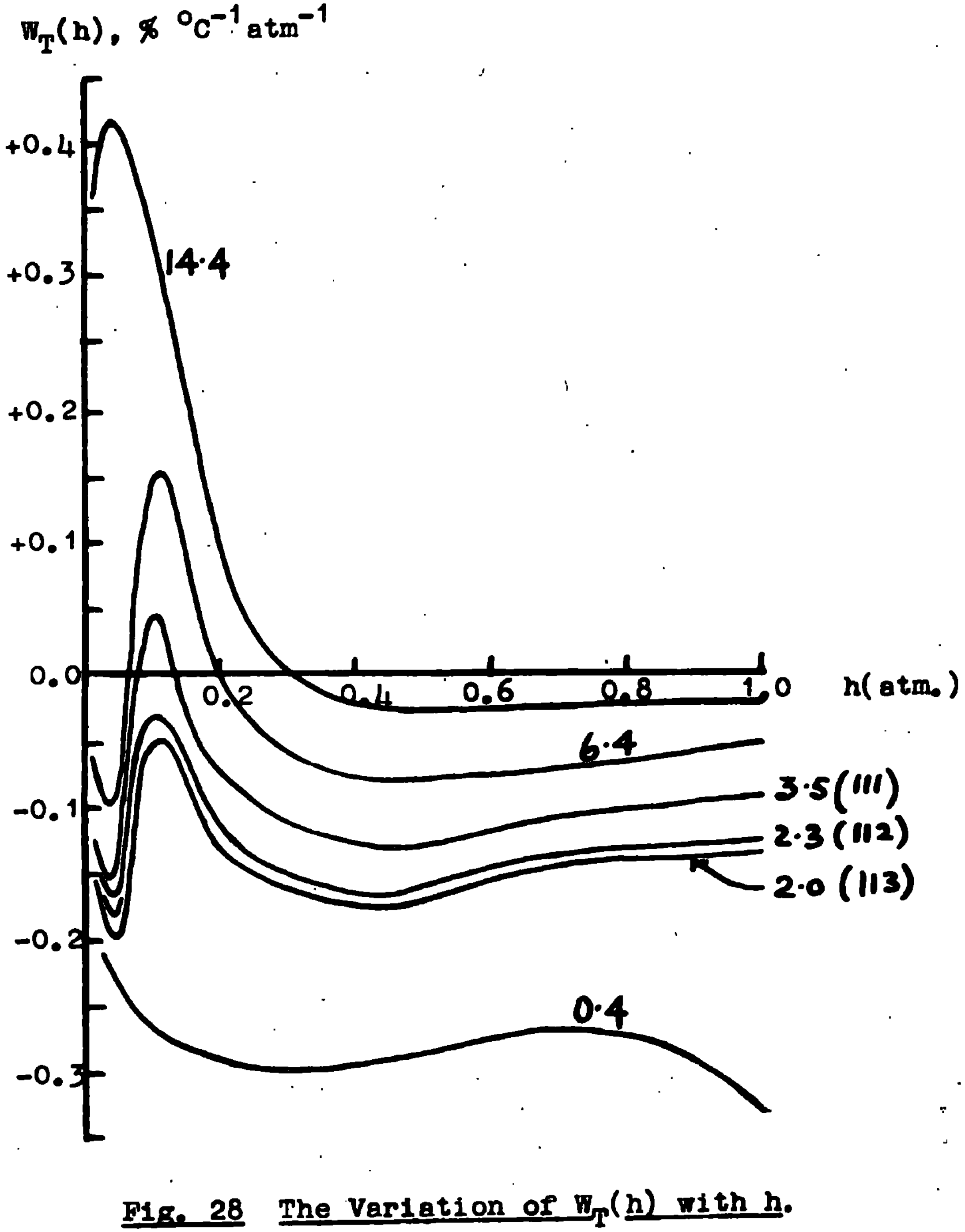

Fig. 28 The Variation of $W_T(h)$ with h.

required for other values of $\Delta \ell$, these are equivalent minimum values for each of the momentum categories, and are:

2.0 GeV for categories 113 and 220
2.3 GeV for categories 112 and 110
3.5 GeV for category 111.

Values of $W_t(h)$ were found by interpolation on a graph of $W_t(h)$ against $\Delta \ell$ with h as parameter and the results are shown in Fig. 28.

The integral can be reqritten, to sufficient accuracy, as

$$\frac{\delta N_\mu}{N_\mu} = \sum_{h=0.1}^{h=1} W_T(h) \Delta T \Delta h = \phi$$

where $\Delta h = 0.1$ atmosphere and ΔT is the difference in temperature of the layer (h) from its mean value. Applying this to the present experiment ϕ was computed from the meteorological data, interpolating the temperature values where necessary, for each category. The intensities were then plotted against ϕ for narrow bands of pressure. A range of values of ϕ was then taken and the mean intensity was then plotted against ϕ for each pressure band. These curves were then normalized to the same mean value to give a master curve of 'mean' intensity against ϕ for each category.

It was found that the resulting 'curve', composed of normalized intensities, showed large fluctuations from one value of ϕ to the next. In many cases the fluctuations were greater than could be accounted for by statistical errors and it was not possible to verify the predicted variation of ϕ.

However, an approximate corrected pressure coefficient was computed for each category, as follows. The data referred to above, on the range of values of ϕ for each pressure band, was taken and the intensities were normalized so that intensity was the same for each band of ϕ. The mean of these corrected intensities was then taken for each pressure band and plotted against pressure and the 'corrected' coefficient determined as described in §8.2. This method is not exact, but is thought to be more accurate than the first approximation. Essentially, it assumes that the temperature effects have the form predicted by Dorman but that the magnitude may be different. The resulting values of α_p, which show rather large errors, are given in Fig. 29. It will be seen that they are systematically below the theoretical curve.

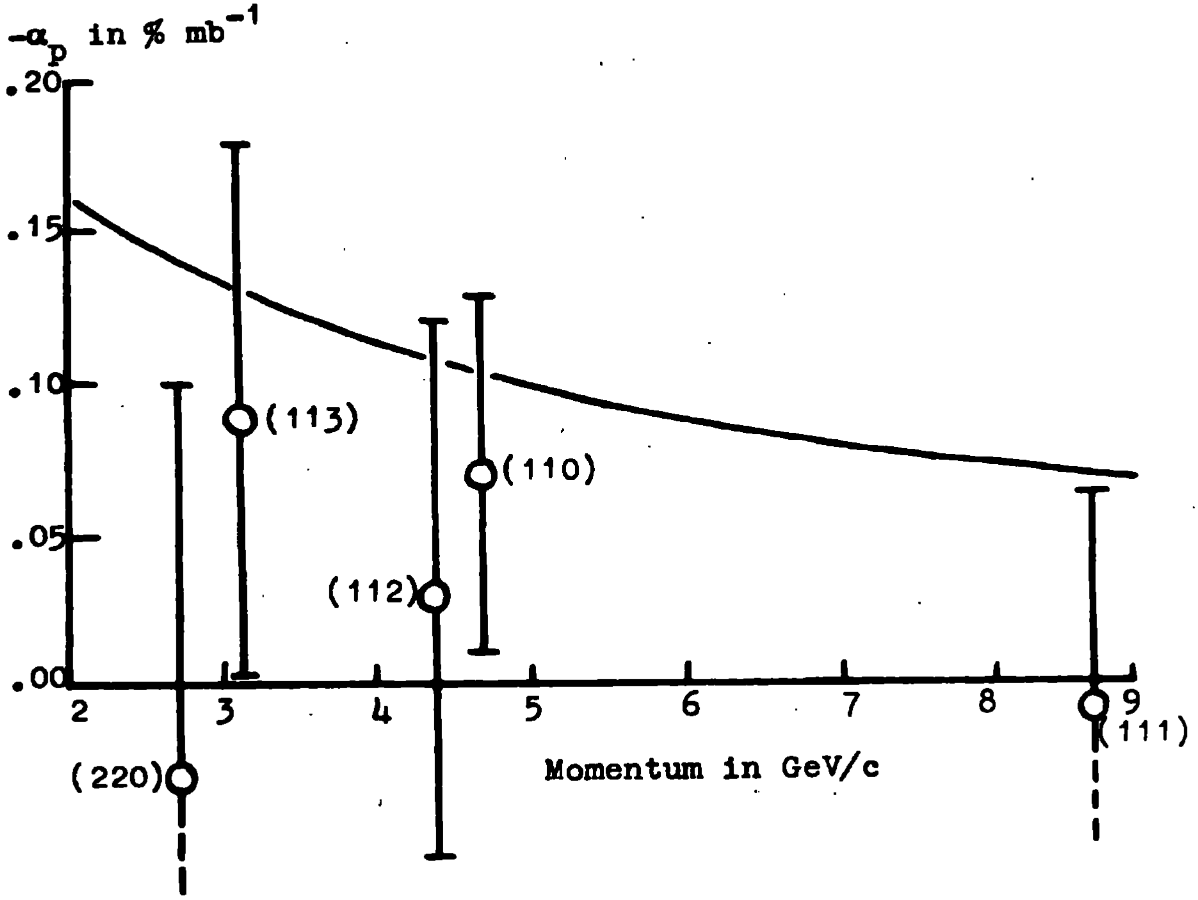

Corrected values of α_p as a function of momentum

Fig. 29

8.4 Conclusions

The conclusions of these experiments on the correlation of the intensity variations with meteorological parameters can be summarized as follows:

1. When the effect of temperature variations is ignored the pressure coefficients are higher than expected by about 70%.
2. The statistical accuracy of the data is too low to allow an accurate correction to be applied for the effect of temperature variations. However, when a very approximate correction is made, the resulting pressure coefficients appear to be too low but the accuracy is so poor that consistency with the expected values cannot be ruled out.

The result is that there is no evidence in favour of any gross discrepancy between the experimental and theoretical values of the pressure coefficient of μ-mesons at ground level in the momentum range 2-10 GeV/c.

Acknowledgments

The Author wishes to thank the Air Research Development Council of the United States Air Force without whose financial assistance the work could not have been done. He is indebted to Professor G.D. Rochester, F.R.S. for the use of his laboratory facilities; to his supervisor Dr. A.W. Wolfendale for his unfailing guidance; to Dr. W.F. Nash of Nottingham University and Mr. H.W. Bennett of Loughborough College of Advanced Technology for many useful discussions. Finally he is indebted to his fellow research students and to the laboratory staff of the Physics Department, especially Mr. E. Anderson whose assistance was invaluable.

REFERENCES

1. O'CONNOR, P.V., and WOLFENDALE, A.W., 1960,
   Suppl. Nuovo Cimento, 15, 202.
2. BENNETT, H.W., and NASH, W.F., 1960,
   Suppl. Nuovo Cimento, 15, 193.
3. ELLIOT, H., 1952,
   Progress in Cosmic Ray Physics, 455.
4. SARABHAI, V., NERURAR, N.W., and BHAVSAR, P.D., 1953,
   Proc. Indian Acad. Sci. A, Vol 41, No. 6, 245.
5. DORMAN, L.I., 1957,
   Cosmic Ray variations, State Publishing House, Moscow.
6. MYSSOWSKY, L., and TUWIM, L., 1927,
   Zeits. f. Phys. 44, 4-5, 369.
7. DUPERIER, A., 1949,
   Proc. Phys. Soc. A62, 684.
8. BACHELOT, F., and CONFORTO, A.M., 1956,
   Nuovo Cimento (Sev. 10), Vol4, No. 6, 1479.
9. OLBERT, S., 1953,
   Phys. Rev., 92, 454.
10. OLBERT, S., 1955,
    Phys. Rev. 96, 1400
11. MATTHEWS, P.M., 1959,
    Canad. J. Phys., Vol 37, No. 2, 85.

12. GLASER, D.A., HAMERMESH, B., and SAFONOV, G., 1950,
Phys. Rev. 80, 625.

13. OWEN, B.G., and WILSON, J.G., 1955,
Proc. Phys. Soc. A68, Pt 5, 409.

14. ASHTON, F., ET AL., 1960,
Nature Vol. 185, 364.

15. ROSSI, B., 1931,
Nature Vol 128, 300.

16. BERNARDINI, G., ET AL., 1945,
Phys. Rev., 68, 109.

17. CONVERSI, M., PANCINI, E., and PICCIONI, O., 1945,
Phys. Rev., 68, 232.

18. BENNETT, H.W., 1960,
M.Sc., Thesis, Nottingham University.

19. MARGERISON, T.A., and SUCKSMITH, W., 1946,
J. Sci. Instrum., 23, 282.

20. HECKSTALL-SMITH, H.W., 1932,
Intermediate Electrical Theory.

21. GARDNER, M., KISDNASAMY, S., RÖSSLE, E., and
WOLFENDALE, A.W., 1957,
Proc. Phys. Soc. B, Vol 70, Pt 7, 687.

22. LLOYD, J.L., and WOLFENDALE, A.W., 1955,
Proc. Phys. Soc. A, Vol 68, Pt 11, 1045.